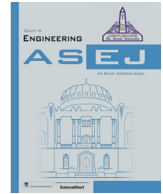




Contents lists available at ScienceDirect

Ain Shams Engineering Journal

journal homepage: www.sciencedirect.com



## State-of-the-Art of the most commonly adopted wave energy conversion systems

Ahmed Mahdy<sup>a</sup>, Hany M. Hasanien<sup>a,b</sup>, Shady H. E. Abdel Aleem<sup>c</sup>, Mujahed Al-Dhaifallah<sup>d,e</sup>, Ahmed F. Zobaa<sup>f,\*</sup>, Ziad M. Ali<sup>g,h</sup>

<sup>a</sup> Electrical Power and Machines Department, Faculty of Engineering, Ain Shams University, Cairo 11517, Egypt

<sup>b</sup> Electrical Engineering Department, Faculty of Engineering and Technology, Future University in Egypt, Cairo 11835, Egypt

<sup>c</sup> Department of Electrical Engineering, Institute of Aviation Engineering and Technology, Giza 25152, Egypt

<sup>d</sup> Control and Instrumentation Engineering Department, King Fahd University of Petroleum & Minerals, Dhahran 31261, Saudi Arabia

<sup>e</sup> Interdisciplinary Research Center (IRC) for Renewable Energy and Power Systems, King Fahd University of Petroleum & Minerals, KFUPM Box 120, Dhahran 31261, Saudi Arabia

<sup>f</sup> Electronic and Electrical Engineering Department, Brunel University London, Uxbridge, U.K

<sup>g</sup> Electrical Engineering Department, College of Engineering at Wadi Addawaser, Prince Sattam bin Abdulaziz University, Wadi Addawaser 11991, Saudi Arabia

<sup>h</sup> Electrical Engineering Department, Aswan Faculty of Engineering, Aswan University, Aswan 81542, Egypt

### ARTICLE INFO

#### Article history:

Received 4 April 2023

Revised 5 May 2023

Accepted 19 May 2023

Available online xxxx

#### Keywords:

Archimedes Wave Swing

Oyster

Oscillating Water Column

Pelamis

Wave Dragon

Wave energy conversion system

### ABSTRACT

The vast diversity of wave energy conversion systems (WECSs) in the literature makes selecting the suitable WECS for wave energy harvest a stubborn process. This work summarizes six of the most widely adopted WECSs used heavily in previous research assessments and practical projects. This includes the Archimedes Wave Swing (AWS), the Wave Dragon (WD), Pelamis Wave Power (PWP), Aquabouy (AB), the Oyster, and the Oscillating Water Column (OWC). The work includes the mathematical modeling of these WECSs and the different projects and prototypes that involve these WECSs. Moreover, the latest research development in each of these WECSs is presented. Also, the wave energy potential in the world is discussed. Besides, the wave energy potential in Egypt, including that of the Mediterranean and the Red Sea, is discussed in detail. Furthermore, the steps required to perform a future feasibility study in Egypt and suggestions for the enhancement of an older study are provided. Finally, some suggestions and required equations are presented to explore the site power density and the most suitable WECS to be utilized in Egypt.

© 2023 THE AUTHORS. Published by Elsevier BV on behalf of Faculty of Engineering, Ain Shams University. This is an open access article under the CC BY license (<http://creativecommons.org/licenses/by/4.0/>).

**Abbreviations:** AGWO, CS Augmented grey wolf optimizer and cuckoo search; AB, Aquabouy; BOWC, Breakwater oscillating water column; CALM, Catenary anchor leg system; COA, COOT optimization algorithm; EMA, Egyptian meteorological authority; EMEC, European marine energy center; GA, Genetic algorithm; HPA, High-pressure accumulator; IMPC, Improved model predictive control; INCOIS, Indian national center for ocean information services; LCOE, Levelized cost of energy; LPA, Low-pressure accumulator; MS, The mediterranean sea; MMB, Multiport magnetic bus; MPC, Model predictive control; NREA, New and Renewable Energy Authority; OWC, Oscillating water column; PCC, Point of common coupling; PTO, Power take-off; PSO, Particle swarm optimization; PWP, Pelamis wave power; RS, The red sea; SALM, Single anchor leg mooring; SSA, Salp swarm algorithm; TENG, Triboelectric nanogenerator; WATERS, Scottish wave and tidal energy: research, development, and demonstration support; WD, Wave dragon; WCA, Water cycle algorithm; WECS, Wave energy conversion system.

\* Corresponding author.

E-mail addresses: [ahmedmahdy@khadijaacademy.com](mailto:ahmedmahdy@khadijaacademy.com) (A. Mahdy), [hanyhasanien@iee.org](mailto:hanyhasanien@iee.org) (H.M. Hasanien), [engshady@iee.org](mailto:engshady@iee.org) (Shady H. E. Abdel Aleem), [mujahed@kfupm.edu.sa](mailto:mujahed@kfupm.edu.sa) (M. Al-Dhaifallah), [azobaa@iee.org](mailto:azobaa@iee.org) (A.F. Zobaa), [dr.ziad.elhalwany@aswu.edu.eg](mailto:dr.ziad.elhalwany@aswu.edu.eg) (Z.M. Ali).

<https://doi.org/10.1016/j.asej.2023.102322>

2090-4479/© 2023 THE AUTHORS. Published by Elsevier BV on behalf of Faculty of Engineering, Ain Shams University.

This is an open access article under the CC BY license (<http://creativecommons.org/licenses/by/4.0/>).

Please cite this article as: A. Mahdy, H.M. Hasanien, Shady H. E. Abdel Aleem et al., State-of-the-Art of the most commonly adopted wave energy conversion systems, Ain Shams Engineering Journal, <https://doi.org/10.1016/j.asej.2023.102322>

### 1. Introduction

Currently, wave energy is at a development crossroads. The power density is the main reason for adopting wave energy over solar and wind. The power density of the wave energy far exceeds the corresponding values in wind and solar. However, the high costs and low maturity of the WECSs led to difficulty in exploiting the wave resource's real potential. To compare these sources, the levelized cost of energy (LCOE) is one of the finest measures for assessing the cost of energy resources; it ranges from 0.18 to 0.87 dollars per kilowatt-hour (k Wh) for WECSs, compared to 0.06–0.38 dollars per k Wh for solar energy and 0.10–0.56 dollars per k Wh for offshore wind energy [1]. This concludes that the LCOE of various wave energy systems is significantly higher. Mainly, the wave energy systems' high cost is because these systems are operated in the ocean environment. These systems should withstand biochemical degradation, the extreme wave forces and

**Nomenclature**

|                       |  |                    |   |
|-----------------------|--|--------------------|---|
| $A_i$                 | $i$ component's amplitude  | $H$                | Wave height   |
| $A_1$                 | Chamber area   | $h_{a0}$           | Height of the chamber top covers the still water level                    |
| $A_2$                 | Orifice area   | $H_i$              | Elevation of the wave $i$   |
| $A_n$                 | The action areas of the $n$ th chamber   | $h_f$              | Floater height  |
| $A_w$                 | Floater plan area  | $H_s, H_m, H_{m0}$ | Significant wave height   |
| $A(\infty), a_\infty$ | Additional mass matrix   | $h(\tau)$          | Retardation function  |
| $b$                   | Viscous damping  | $I$                | The body's moment of inertia  |
| $B$                   | Air damping  | $I_\infty$         | The added moment of inertia   |
| $B_{cush}$            | Cushion damping coefficient  | $i_{abc}$          | 3-phase currents  |
| $B_m$                 | Hydraulic motor and couplings rotational damping                               | $i_d \& i_q$       | $dq$ stator currents  |
| $B_{nl}$              | Viscous damping coefficient  | $I_5$              | The buoy moment of inertia around the $y$ -axis                           |
| $\beta_e$             | The oil bulk modulus   | $J$                | Average energy flux per unit crest  |
| $\beta_g$             | Generator damping coefficient  | $J_m$              | Hydraulic motor and couplings rotational inertia                          |
| $\beta_{wb}$          | Coefficient of the water brakes  | $k$                | Wave number   |
| $c$                   | PTO spring stiffness   | $K$                | Radiation impulse response function                                       |
| $C_D$                 | Drag coefficient   | $K_e$              | Surface elevation to the torque impulse response                          |
| $C_d$                 | Coefficient of discharge   | $K_{hys}$          | Hydrostatic recovery stiffness matrix                                     |
| $C_{DDW}$             | Drag coefficient of downwards motion   | $K_{hr}$           | Hydrostatic restoring coefficient   |
| $C_{DUP}$             | Drag coefficient of upwards motion   | $k_p$              | Pitch stiffness   |
| $C_g$                 | Group celerity   | $K_{pw}$           | Waves' decay factor   |
| $c_M$                 | Inertia coefficient  | $K_1$ and $K_2$    | Flow coefficients in PWP  |
| $d$                   | Wet surface length of the chamber at still water level                         | $k_s$              | Spring constant   |
| $d_f$                 | The floater depth at mid-position  | $L$                | Inductance matrix   |
| $d_p$                 | PTO system damping   | $L_d$ and $L_q$    | The $d$ -axis and the $q$ -axis inductances                               |
| $d_{out}$             | The cylinder's outer diameter  | $L_{eq}$           | Spring length at equilibrium  |
| $\Delta\omega_i$      | Interval of wave frequency   | $L_s$              | Synchronous inductance  |
| $\Delta P(t)$         | Difference in pressure between inside the chamber and the atmospheric pressure | $L_{ss}$ and $M$   | Phase self and mutual inductances between two stator phases, respectively |
| $\eta_{tl}$           | Tide level   | $\lambda_{ge}$     | Generator pole width  |
| $\eta(t)$             | The sea waves' elevation   | $m$                | Buoy mass   |
| $\varepsilon$         | Water surface elevation  | $M$                | Mass of the water column at the still water level                         |
| $\psi_{PM}, \psi_f$   | Permanent magnet's flux linkage  | $M_a$              | Added mass  |
| $\psi_{PM-abc}$       | Flux linkage matrix of the stator  | $M_1$              | Floater mass  |
| $F$                   | Total force  | $M_2$              | The water mass in the accelerator tube                                    |
| $f(t)$                | Total forces acting on the water column  | $M_b$              | Mass matrix   |
| $F_{Air}$             | Air pressure force   | $m_{-1}$           | The wave spectrum's minus first moment                                    |
| $F_{drag}$            | Water's drag force   | $m_0$              | The wave spectrum's zeroth moment   |
| $F_{grav}$            | The gravitational force  | $m_n$              | The $n$ th spectral moment  |
| $F_{bear}$            | Frictional force affecting the AWS bearings                                    | $m_{add}$          | Added mass  |
| $F_{Horizontal}$      | Horizontal force affecting the AWS bearings                                    | $m_f$              | Floater mass  |
| $F_{ff}$              | Fluid friction force   | $m_t$              | Total mass  |
| $F_{hS}$              | Force of the hydrostatic pressure  | $\mu$              | Coefficient of the bearing friction                                       |
| $F_{Nitro}$           | Nitrogen cylinder force  | $N$                | Number of waves   |
| $F_{rad}$             | Radiation force because of the floater's oscillation inside the water          | $N_p$              | Generator rotor pole number   |
| $F_{sp}$              | Force of the spring because of the gas pressure in the AWS                     | $L$                | Incident wavelength   |
| $F_{sp-eq}$           | Spring force at equilibrium  | $L_c$              | Single chamber length   |
| $F_{hS-eq}$           | Force of the hydrostatic pressure at equilibrium                               | $\omega$           | Angular wave frequency  |
| $F_{wb}$              | Water brakes force   | $\omega_{gen}$     | Voltage angular speed   |
| $F_{end}$             | Force generated in case the floater hits the end stops                         | $\omega_i$         | The wave $i$ angular frequency  |
| $F_e, F_w(t)$         | The waves' excitation force  | $\omega_n$         | Angular tuning frequency  |
| $F_{ex}^1$            | Buoy force in the surge mode   | $P$                | LPMSG real power  |
| $F_{ex}^2$            | Buoy force in the heave mode   | $P_{abs}$          | Absorbed power by the PTO   |
| $F_{generator}$       | Generator applied force  | $P_c$              | Instantaneous chamber pressure  |
| $F_{FK}(t)$           | Froude- Krylov force   | $P_{cs,B,a}$       | WD main body's absorbed power   |
| $F_a(t)$              | The damping force of the added mass  | $P_{cs,R,i}$       | Total available wave power between the cross-section of the reflectors    |
| $F_{\Delta p}(t)$     | Variation of the air force   | $P_{dB}$           | The energy flux integrated from the body's draft up to the surface        |
| $\{F_m(t)\}$          | Hydraulic motor force matrix   | $P_{wave}(t)$      | Dynamic pressure field  |
| $\{F_{ex}(t)\}$       | Excitation force matrix  | $q$                | Overtopping rate  |
| $\{F_{pto}(t)\}$      | PTO force matrix   | $q_n$              | The flow of the $n$ th valve  |
| $F_{pto}$             | PTO force  | $q_N$              | Non-dimensional overtopping rate  |
| $g$                   | Gravitational acceleration   | $R$                | Three-phase resistance vector   |
| $\gamma$              | Heat capacity ratio or the adiabatic exponent                                  | $R(t)$             | Hysteresis function   |
| $h$ and $d$           | Depth to seabed and depth of floater, respectively                             | $R_c$              | Crest freeboard   |

|               |   |                   |  |
|---------------|---|-------------------|--|
| $R_g$         | Ideal gas constant                        | $\theta$          | Flap rotation  |
| $R_t$         | Damping coefficient of $F_{rad}$          | $\theta_c$        | Chamber angular length   |
| $\rho$        | Water density                             | $\theta_e$        | Position of the end stop   |
| $p_{amp}$     | Ambient pressure                          | $\theta_i$        | The wave $i$ phase shift   |
| $p_n$         | The pressure of the $n$ th chamber        | $\theta_t$        | The frames conversion angle  |
| $S(\omega_i)$ | Component $i$ spectral density            | $\theta_m$        | Wave direction   |
| $\sigma$      | Violation in the vertical displacement    | $u$ and $\dot{u}$ | Horizontal velocity and acceleration of the wave-current, respectively |
| $S_{hs}$      | Hydrostatic stiffness                     | $v$               | Velocity of the floater  |
| $S_f$         | Floater's outer area                      | $v_{abc}$         | 3-phase voltages   |
| $S_f$         | Floater's inner area                      | $v_d \& v_q$      | $dq$ stator voltages   |
| $T$           | Incident wave period                      | $V_{DCL}$         | DC link voltage  |
| $T_c$         | Hydraulic motor Coulomb resistance torque | $V_n$             | Volume of the $n$ th chamber of the hydraulic cylinders in PWP         |
| $T_e$         | Wave period                               | $v_n$             | Speed of the $n$ th chamber  |
| $T_{ex}^3$    | Buoy action torque in the pitch mode      | $V_{PCC}$         | Voltage of the point of common coupling                                |
| $T_{elec}$    | Generator torque                          | $V_B$             | Ramp width   |
| $T_k$         | Ambient temperature in Kelvin             | $x$               | AWS floater vertical displacement                                      |
| $T_m$         | The hydraulic motor driving torque        | $x_{eq}$          | Equilibrium position of the spring                                     |
| $T_n$         | AWS Tuning frequency                      | $X_s$             | Synchronous reactance  |
| $T_p$         | The peak energy density's wave period     | $Z_G$             | Buoy gravity coordinates   |
| $T_{PTO}(t)$  | Torque of the PTO                         |                   |  |
| $T_w(t)$      | Incident wave torque                      |                   |  |

ensure a secure connection to the power grid. All of these factors force the stakeholders and the developers to improve the economic feasibility of the WECSs to be able to compete with other developed mature resources like fossil fuels, solar, and wind. The concepts of wave energy conversion system (WECS) design are profuse, and there is no one general unique design agreed on. Hence, one can find in the literature hundreds of WECSs that lead to difficulty in selecting the suitable WECS.

In the literature, several previous reviews discussed the potential and applications of WECSs [2], the layout optimization strategies [3], the tidal current energy converters [4], the performance assessment of WECSs in the highest power density locations [5], and WECS array layout optimization [6]. Unfortunately, one cannot find one comprehensive review that provides the most commonly adopted WECSs with the latest research, projects, prototypes, and modeling. This work fills this gap by describing six of the most widely adopted WECSs used heavily in previous research assessments and practical projects. This includes the Archimedes Wave Swing (AWS), the Wave Dragon (WD), Pelamis Wave Power (PWP), Aquabouy (AB), the Oyster, and the Oscillating Water Column (OWC). This work only lacks the different control systems utilized by these WECSs [7], the environmental impacts of these WECSs [8], the enhancement in the geometric shapes of WECSs [9], the installation and running costs of these WECSs compared to other renewable and non-renewable energy sources, and the systematic approach for selecting the WECSs [10].

The strategy followed to obtain the WECSs data is illustrated in Fig. 1. First, a search is performed on Scopus to find the different assessments of wave energy worldwide. The search is limited to the subject areas: "Energy" and "Engineering." Then, the number of times different WECSs were used in these assessments was counted. The top-mentioned WECSs are selected for review. Moreover, a search was performed for each WECS on Scopus to ensure a heavy demand for this WECS. For example, the Oscillating Water Column was mentioned only four times in the assessments. However, more than 827 research works on Scopus contain the keyword "Oscillating Water Column Wave Energy Converter." That's why this WECS must be included in the review. Second, a search was performed on Scopus, Google Scholar, and the company website to obtain the projects and prototypes for this WECS. Third, a summary of the latest research in the last five or ten years was discussed in detail. This includes the main goal and the contribution

of each research work. If there are many research works, the most cited ones were selected instead. Finally, the mathematical modeling of each WECS was obtained by searching for relevant papers on Scopus.

Unfortunately, some challenges need to be considered in future research. This includes:

1. WECSs must survive extreme sea conditions, which leads to the high cost of WECSs. The challenge is to enhance the design WECSs and build them at a lower price and simultaneously with an excellent ability to survive strong sea waves.
2. The WECS components, including force, speed, and displacement, are designed to provide nominal power at certain conditions. However, as the operating conditions move away from nominal values, the WECS loses its efficiency. Therefore, more research should be performed to enhance the energy harvest under non-optimal conditions [11].
3. The enhancement of the energy harvest at non-optimal conditions can be achieved by improving the control system of the WECS. As an example for AWS WECS, controlling the quadrature axis current leads to controlling the force of the electrical generator and achieving much higher power than without control case. The same principle should be applied to other types of WECSs to maximize the energy yield.
4. The output power of the WECSs has high fluctuations between nominal and peak values due to the high variability of the wave power resource. These fluctuations in power are much worse than other renewable sources such as wind or solar, making it a challenge that requires additional components such as energy storage systems to provide constant power to the grid.
5. The severe restrictions in the power grid requirements and the high output power variability make it hard for WECSs to satisfy the grid requirements.
6. Simulation models are required for WECSs to investigate the generation potential, the control system performance, and the transient stability. Only grid-connected simulation models exist in the literature for AWS and WD WECSs. However, the literature lacks models for other WECSs.

Solving these challenges will make wave energy conversion systems competitive in the market. In addition, more utilization of

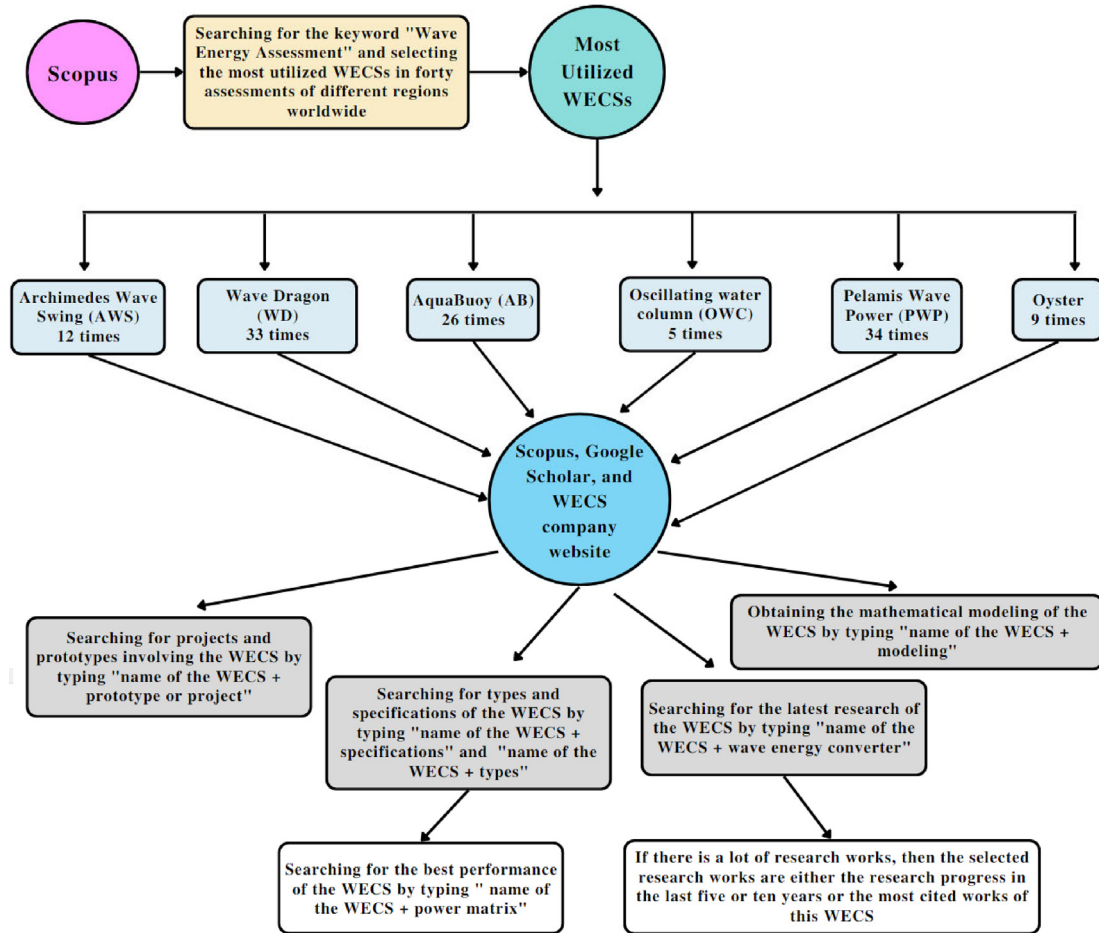


Fig. 1. Strategy followed in the literature review.

these WECSs will help reduce the global warming crisis due to carbon emissions and satisfy the world's future demand for electricity.

The contribution of this work can be summarized as follows:

- 1- The mathematical modelling of six WECSs: the Archimedes Wave Swing (AWS), the Wave Dragon (WD), Pelamis Wave Power (PWP), Aquabouy (AB), the Oyster, and the Oscillating Water Column (OWC) are described in detail.
- 2- The different projects and prototypes involving these WECSs are presented.
- 3- The latest research development regarding these converters is also described.
- 4- A complete comparison between the six WECSs is performed.
- 5- The wave energy potential in the world and Egypt is discussed in the work.
- 6- The steps for performing a future feasibility study in Egypt to observe the generation potential of these WECSs were provided in addition to the enhancement of an old study.

This work is organized as follows: The types of WECSs discussed are presented in Section II. Section III discusses the Archimedes Wave Swing WECS. Section IV describes the Wave Dragon WECS. The Pelamis Wave Power WECS is presented in Section V. Section VI represents the AquaBuoy WECS. Also, Section VII discusses the Oyster WECS. The Oscillating Water Column is presented in Section VIII. In addition, Egypt's wave energy potential and the steps for a feasibility study are represented in Section IX. Lastly, the conclusion is introduced in Section X.

## 2. Types of wave energy conversion systems (WECSs)

More than 1000 WECSs were developed to convert sea waves into useful electrical energy. These WECSs can be classified into six main categories: submerged pressure differential, point absorbers, overtopping devices, oscillating water column, oscillating wave surge converters, and attenuators. After analyzing 40 assessments for wave energy resources, the most utilized WECSs were selected for the review. The main categories and the selected WECSs are shown in Fig. 2 [12,13].

## 3. Archimedes wave Swing (AWS)

In this section, the essential points of AWS are discussed, in addition to the projects and prototypes involving the AWS WECS. Moreover, the latest research regarding AWS is discussed in detail. Finally, the mathematical modelling of the AWS including the linear and nonlinear models is presented.

### 3.1. Introduction to AWS

AWS is a completely submerged WECS. It converts the vertical motion of its floater because of the sea waves into usable electrical power. The conversion is achieved using a permanent magnet synchronous generator. This WECS can be installed in depths greater than 25 m [14]. The most important points of this WECS are illustrated in Fig. 3 [15,16].

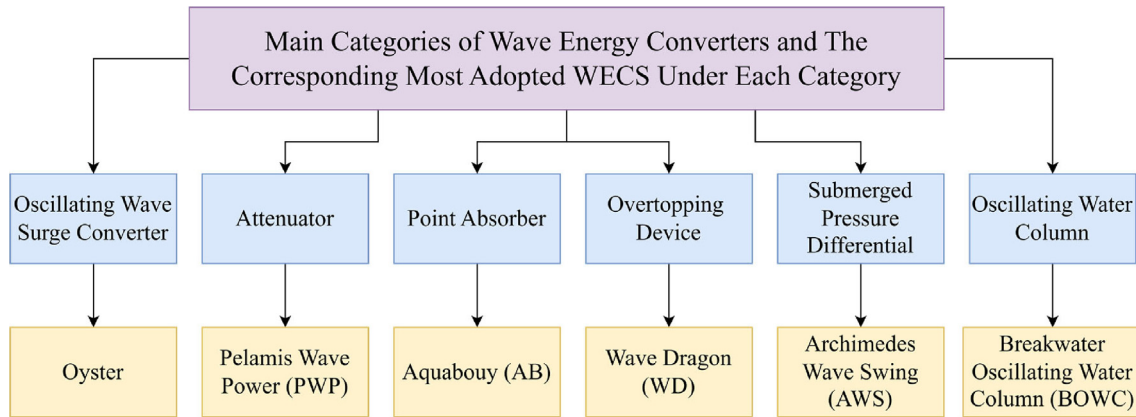


Fig. 2. An overview of types of WECSs.

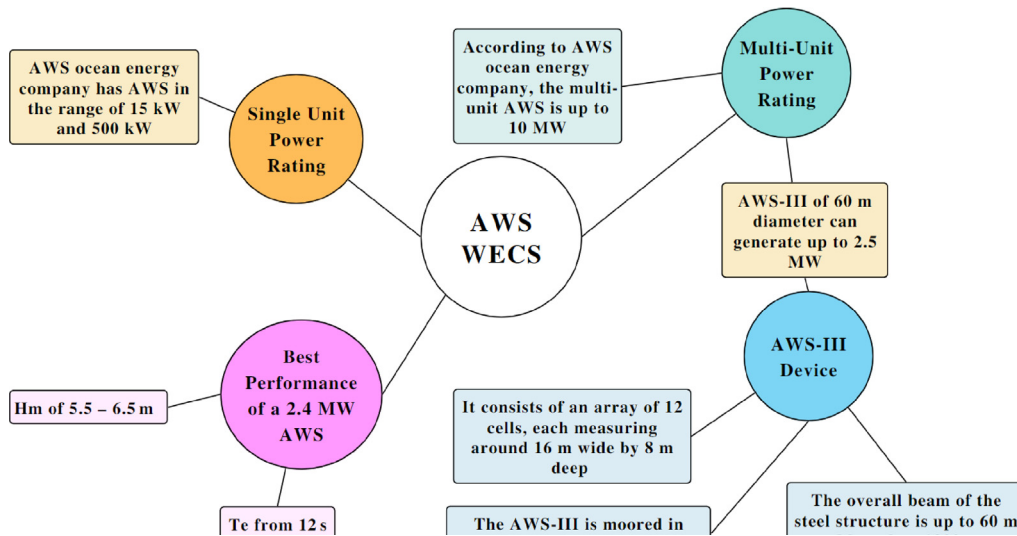


Fig. 3. An overview of AWS WECS.

In Fig. 3,  $T_e$  and  $H_m$  are the wave period and the significant wave height, respectively.

3.2. AWS projects and prototypes

There are several projects involving AWS WECS and prototypes for testing AWS. A summary of these projects and prototypes is shown in Table 1.

3.3. AWS research progress

On Scopus, there are currently 81 research papers about AWS. This work performed detailed research on the latest work about AWS in the last five years. The most important research works are represented in Table 2.

3.4. AWS linear and nonlinear models

In this section, the mathematical modelling of both the linear model and nonlinear model of the AWS WECS is presented. This will help in understanding the importance of utilizing the nonlinear model and why it expresses the actual generation potential of the AWS.

Table 1  
AWS's Projects and Prototypes.

| Reference Number | Year | Summary of the project or prototype  |
|------------------|------|--|
| [17,18,19]       | 2004 | An AWS pilot plant of a 2 MW power was submerged at the Leixões harbor in Portugal. The floater was 9.5 m in diameter and 21 m in height, with a rated stroke of 7 m and 206 tons.   |
| [20]             | 2010 | In Loch Ness, an AWS-III (1:9 scale model) was tested.   |
| [21]             | 2012 | A 50-kW linear C-GEN prototype manufactured by Fountain Design Ltd was built and tested in the U.K. The machine had a stroke of 2 m. The optimized linear generator for the AWS had an 87.5% average efficiency.   |
| [22,23]          | 2012 | The Costa head wave project: A 200 MW of AWS-III wave energy converters was planned to be installed approximately 5 km north of Orkney Mainland by Alstom and SSE Renewables. An initial phase of around 10 MW is installed before the whole site capacity is installed. In 2012, full-scale testing of the components was performed with the help of the Scottish Wave and Tidal Energy: Research, Development, and Demonstration Support (WATERS). In 2014, a full-scale prototype was planned to be deployed. However, no update about this project is available. |

**Table 2**  
AWS's Latest Research Work.

| Reference Number | Year | Summary of the research work   |
|------------------|------|--|
| [24]             | 2018 | The dynamic performance of a hybrid grid-connected WECS consisting of two AWS WECSs and a Wells turbine was analyzed. The two AWS are connected to two linear generators, and the Wells turbine drives a squirrel-cage rotor induction generator. The two AWS are connected to the grid via two generator-side converters and one grid-side converter. Notably, the air turbine or the Wells turbine is unidirectional regardless of the airflow direction [25]. An oscillating air current is formed in the oscillating water column (OWC) WECS due to seawater's rising and falling. Using a Wells turbine eliminates the requirement of any expensive check valves. This reduces the overall cost of the system.  |
| [26]             | 2019 | This paper's main objective is to model the AWS for wave energy harvest from the Indian Ocean. To analyze the output power from the AWS, the authors used the data collected by the Indian National Centre for Ocean Information Services (INCOIS). The government obtained data from different locations using a Moored Buoy that measures $T_e$ and $H_m$ . The authors enhanced the energy harvest by increasing the orifice area by 95%. The result is an increase in the model's output power from 2.39 to 26.50 kW.  |
| [27]             | 2019 | A decoupled model for AWS was built to investigate the chaos phenomenon in the WECS. It was found that during operation, the WECS may be chaotic. The disengagement of the WECS from the chaotic state was achieved using a sliding mode controller. Also, a back propagation neural network was adopted to fit the global control under various control parameters of the sliding mode controller. In addition, the control parameters were selected using particle swarm optimization (PSO). Finally, the results showed that the system robustness was improved, the overshoot was suppressed, and the response time was reduced.   |
| [28]             | 2019 | A complete grid-connected model for AWS was built using the PSCAD program. The system consisted of two converters for grid connection. The first converter minimizes the generator losses and extracts the wave's largest power. These functions were achieved by controlling the direct axis ( $I_d$ ) and quadrature axis ( $I_q$ ) currents of the generator. The second converter controlled the DC link voltage ( $V_{DC}$ ) and the voltage of the point of common coupling ( $V_{PCC}$ ). In addition, the water cycle algorithm (WCA) was utilized to optimize all of the PI gains of the whole control system. Finally, the transient stability of the system under different fault conditions was investigated. It was found that the results of the dynamic performance of the WCA were much better than those obtained using GA.   |
| [29]             | 2019 | In this work, a model similar to [28] was built in MATLAB Simulink but with an additional enhancement. In this work, a bidirectional DC-DC converter with a supercapacitor was utilized to keep $V_{DC}$ constant. Also, the grid side converter controlled both the supplied active power and $V_{DC}$ . This helped in smoothing out the fluctuations in the generator power supplied to the grid.   |
| [30]             | 2020 | The structural analysis tool was utilized to perform a fault diagnosis for the AWS during various conditions. The study included damage to the water brakes, faults in the speed and position sensors, fault in the actuator, and perforation in the central tank. The transient analysis of these faults was performed in the MATLAB Simulink.  |
| [31]             | 2020 | The model predictive control (MPC) is utilized instead of the conventional PI controllers to control an AWS WECS connected to a DC microgrid. In this system, the generator side converter contains an MPC to achieve the same functions [28]. Also, similar to [29], the supercapacitor was utilized to preserve $V_{DC}$ at its reference value. Using MATLAB Simulink, the MPC's performance was compared to the conventional PI control system. It was concluded that MPC produced much better results during regular and irregular waves.   |
| [32]             | 2020 | This work presents decentralized power management for an AWS with an islanded microgrid. The control system can be analyzed into three subsystems. The first one manages the power flow between the hybrid system (AWS and a battery) and the microgrid to keep the frequency within the allowable limits. The second one is to yield the highest possible power from sea waves and prevent battery overcharging. The third one is to control the $V_{DC}$ at its reference value. Finally, the system was investigated under different values of the battery's charge state and the microgrid's operating conditions. The control performance of the system was evaluated using MATLAB Simulink.  |
| [33]             | 2020 | Instead of using one AWS, this work presents the usage of a farm of AWS WECSs. This will help eliminate the requirement for an expensive energy storage system. Also, it will provide almost constant power to the electrical grid. In addition, the 42-year data obtained by the buoy near Port Kembla were used to analyze the system's performance. Finally, the flicker level at the point of common coupling (PCC) was evaluated in grids with different strengths. The results confirmed that the system complies with the grid code of several countries.   |
| [34]             | 2021 | This work presents a generation system formed of a wind turbine and a group of AWS WECSs. Also, the back-to-back converter of the WECS is replaced by a high-frequency multipoint magnetic bus (MMB) DC-DC converter. It acts as an isolator between the wind energy system and the AWS WECSs. In addition, it makes the system more compact. Also, a damping controller was utilized to yield the maximum power from sea waves. Also, $V_{DC}$ is regulated using the MMB DC-DC converter. Finally, the results verify the excellent performance of the proposed control.   |
| [35]             | 2021 | This paper represents a combined model that helps forecast sea waves. The waves can be decomposed into wind swells and waves. The model utilizes the improved grey BP neural network to find the correlation between wind speed and wind waves. Then, based on the wind speed data, a forecast for the average wind waves can be achieved. Also, the autoregressive integrated moving average can forecast the average wave height of the swells. Finally, the wave average height can be obtained by combining the wind swell and wave. In addition, the AWS is utilized to generate electricity from sea waves. Finally, the forecast model's effectiveness was validated.   |
| [36]             | 2021 | An improved version of the MPC denoted by IMPC was utilized for a system consisting of a supercapacitor energy storage system that helps provide constant power to a load by stabilizing $V_{DC}$ and a WECS. The control strategy is based on a modified objective function and the incremental generator model to reduce the final steady-state error. The authors found that this control system can preserve the stability of the hybrid system under different loading conditions, including regular and irregular waves and faults. This helped in improving the system's robustness. The results of the IMPC were compared to the conventional MPC. Under the regular waves, the results showed that the $q$ -axis and $d$ -axis errors could be decreased by 50% and 37.5%, respectively. Also, under irregular waves, when one leg loses, the IMPC reduces the $q$ -axis error peak from 73A down to 1.5 A. |
| [37]             | 2022 | The dynamic stability of an AWS was improved using the salp swarm algorithm (SSA) [38]. The grid-connected AWS is similar to that in [28]. The SSA selects the PI gains in the control system using an integral squared error objective function. In addition, the SSA-based PI gains were compared to those obtained using the GA during a severe disturbance in the grid. In addition, the measured wave pressure data obtained by Polinder in the Portugal AWS prototype were applied to the PSCAD model for a more realistic study. The results obtained showed excellent performance of the SSA controllers compared to the GA controllers. These results are verified during symmetrical and unsymmetrical faults. Finally, the system showed good performance under the effect of the irregular waves.  |
| [39]             | 2022 | The transient stability for the same system in [28] was improved using the COOT optimization algorithm (COA) [40]. The PI gains were selected using the COA under the minimum number of iterations compared to previous research works. Moreover, an anti-windup scheme was added to enhance the transient performance of the system. The results showed superior performance due to the addition of the anti-windup compared to the controllers without an anti-windup.   |
| [41]             | 2022 | The authors used an AWS nonlinear model instead of the linearized model implemented in the previous research work. The work provides different reasons why a linearized model is not enough to describe the actual generation behavior of an AWS WECS. Also, the augmented grey wolf optimizer and cuckoo search (AGWO-CS) was utilized to select the PI gains [42]. The results obtained by this algorithm are compared to those obtained from the COA and PSO. The real-time simulation of the system was performed using RT-LAB and OP4510 to evaluate the control system performance. The experimental and simulation results were very close to each other.   |
| [43]             | 2022 | The authors used an AWS nonlinear model parallel with a PV system to supply enough electrical power for a V3 Tesla Supercharging system. Due to the high variability nature of the AWS, the hybrid system is stabilized using a supercapacitor. The control system is composed of seven PI controllers that were tuned using Golden Jackal Optimization Algorithm (GJOA) [44]. The system was subjected to different scenarios including a short circuit and connection of electric vehicles.  |

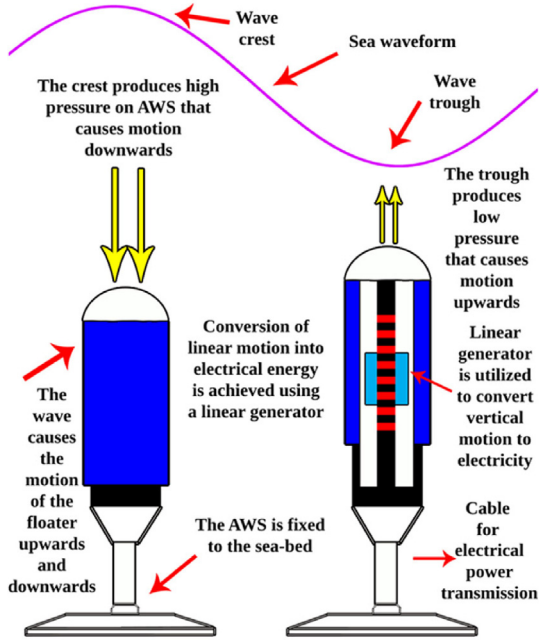


Fig. 4. AWS WECS principle of operation [39].

### 3.4.1. AWS nonlinear model

Since [41] represents a critical enhancement to the modeling of the AWS. The representation of the AWS linear and nonlinear models will be explained in detail. The AWS is illustrated in Fig. 4.

The AWS floater motion can be represented by Eqs. (1) and (2) [19]. A description of these forces will be represented further.

$$m_f \frac{dv}{dt} = F_{drag} + F_{grav} + F_{hs} + F_{rad} + F_{sp} + F_{wb} + F_{gen} + F_{end} + F_e + F_{bear} \quad (1)$$

$$v = \frac{dx}{dt} \quad (2)$$

The first force is the drag force of water, which is denoted by  $F_{drag}$ . This force during positive and negative velocities can be represented according to Morison by Eq. (3) [45]. In this equation, the drag coefficients of upward and downward motions are defined by  $C_{DDW}$  and  $C_{DUP}$ , respectively. Also,  $v$  is the velocity of the floater.

$$F_{drag} = \begin{cases} -\frac{1}{2} \rho S_F v |v| C_{DUP}, & v \geq 0 \\ -\frac{1}{2} \rho S_F v |v| C_{DDW}, & v < 0 \end{cases} \quad (3)$$

$F_{grav}$  is the floater's weight gravitational force.  $F_{grav}$  is represented by Eq. (4). In Eq. (4), the floater's mass, outer area, and gravity acceleration are denoted by  $m_f$ ,  $S_F$ , and  $g$ , respectively.

$$F_{grav} = -m_f g \quad (4)$$

Eq. (5) represents the force of the hydrostatic pressure ( $F_{hs}$ ) [46]. In this equation,

$\eta_{tl}$ ,  $d_f$ ,  $h_f$ ,  $S_f$ ,  $x$ , and  $p_{amp}$  represent the tide level, the floater top depth, the floater height, the floater's inner area, the position, and the ambient pressure, respectively.

$$F_{hs} = -S_f (\rho g (d_f + \eta_{tl} - x) + p_{amp}) + (S_f - S_f) (\rho g (d_f + \eta_{tl} + h_f - x) + p_{amp}) \quad (5)$$

The radiation force ( $F_{rad}$ ) is represented by Eq. (6) [47]. In this equation,  $R(t)$  and  $m_{add}$  are the fluid memory retardation function and the infinite frequency added mass, respectively. This equation can be approximated to Eq. (7), in which,  $R_t$  is a damping coefficient.

$R_t$  can be calculated using Eq. (8). In Eq. (8), the angular tuning frequency and the tuning frequency are represented by  $\omega_n$  and  $T_n$ , respectively.  $\omega_n$  is equal to  $2\pi/T_n$ .

$$F_{rad} = -m_{add} \frac{dv}{dt} - \int_0^t R(t-\tau) v(\tau) d\tau \quad (6)$$

$$F_{rad} = -m_{add} \frac{dv}{dt} - 2R_t v \quad (7)$$

$$R_t = \begin{cases} \omega_n \times 6.4286 \times 10^4 - 8.2143 \times 10^3, & \omega_n < 0.75 \\ 40000, & \omega_n < 0.89 \\ -\omega_n \times 5.2632 \times 10^4 + 8.6842 \times 10^4, & \omega_n < 1.08 \\ -\omega_n \times 7.1429 \times 10^4 + 1.0714 \times 10^5, & \omega_n > 1.08 \end{cases} \quad (8)$$

Eq. (9) represents the spring force ( $F_{sp}$ ). In this equation,  $x_{eq}$ ,  $\gamma$ ,  $F_{sp-eq}$ , and  $L_{eq}$  represent the spring's position, the heat capacity rate, the spring's force, and the spring's length at equilibrium.  $F_{sp-eq}$  is equal to the summation of the hydrostatic force ( $F_{hs-eq}$ ) at equilibrium and  $F_{grav}$ .  $F_{sp-eq}$  is represented by Eq. (10). Finally,  $L_{eq}$  is obtained by Eq. (11).

$$F_{sp} = F_{sp-eq} \left( \frac{L_{eq}}{L_{eq} + x - x_{eq}} \right)^\gamma \quad (9)$$

$$F_{sp-eq} = -F_{hs-eq} - F_{grav} \quad (10)$$

$$L_{eq} = \frac{\gamma F_{sp-eq}}{(\omega_n^2 (m_{add} + m_f) + \rho g S_f)} \quad (11)$$

Eq. (12) represents the water brakes force ( $F_{wb}$ ) that operates when a vertical limit is exceeded. In this equation, the water brakes' coefficient and the violation in vertical displacement are represented by  $\beta_{wb}$  and  $\sigma$ , respectively.

$$F_{wb} = -\beta_{wb} v |v|, x \geq \sigma \text{ or } x \leq -\sigma \quad (12)$$

Eq. (13) represents the end force ( $F_{end}$ ) that operates when the position  $\theta_e$  is reached.

$$F_{end} = -\frac{v(m_{add} + m_f)}{0.1}, x \geq \theta_e \quad (13)$$

The waves excitation force ( $F_e$ ) applied by the waves is calculated using Eq. (14). In this equation, the decay factor of the waves and the final wave elevation is denoted by  $K_{pw}$  and  $\eta(t)$ , respectively.  $\eta(t)$  can be obtained using Eqs. (15), (16), and (17) [48]. In these equations,  $H_i$ ,  $\omega_i$ ,  $\theta_i$ ,  $A_i$ ,  $S(\omega_i)$ , and  $\Delta\omega_i$  represent elevation, angular frequency, phase shift, amplitude, spectral density, and frequency interval of the wave  $i$ , respectively. In addition  $N$ ,  $H_s$ , and  $T_p$  are the number of waves, significant wave height, and the peak energy density's wave period, respectively. Note that  $S(\omega)$  represents the wave spectrum, in this model, the Bretschneider was adopted. Also, the values of  $\omega_i$  and  $\theta_i$  are in the range of [0.5–2.5] rad/s and [0 – 2π] radian. This spectrum is shown in Fig. 5(a).

$$F_e = \rho g S_F \eta(t) K_{pw} \quad (14)$$

$$\eta(t) = \sum_{i=1}^N \frac{H_i}{2} \sin(\omega_i t + \theta_i) \quad (15)$$

$$A_i = \frac{H_i}{2} = \sqrt{2S(\omega_i) \Delta\omega_i} \quad (16)$$

$$S(\omega) = \frac{486 H_s^2}{T_p^4 \omega^5} e^{-\frac{1948.2}{T_p^4 \omega^4}} \quad (17)$$

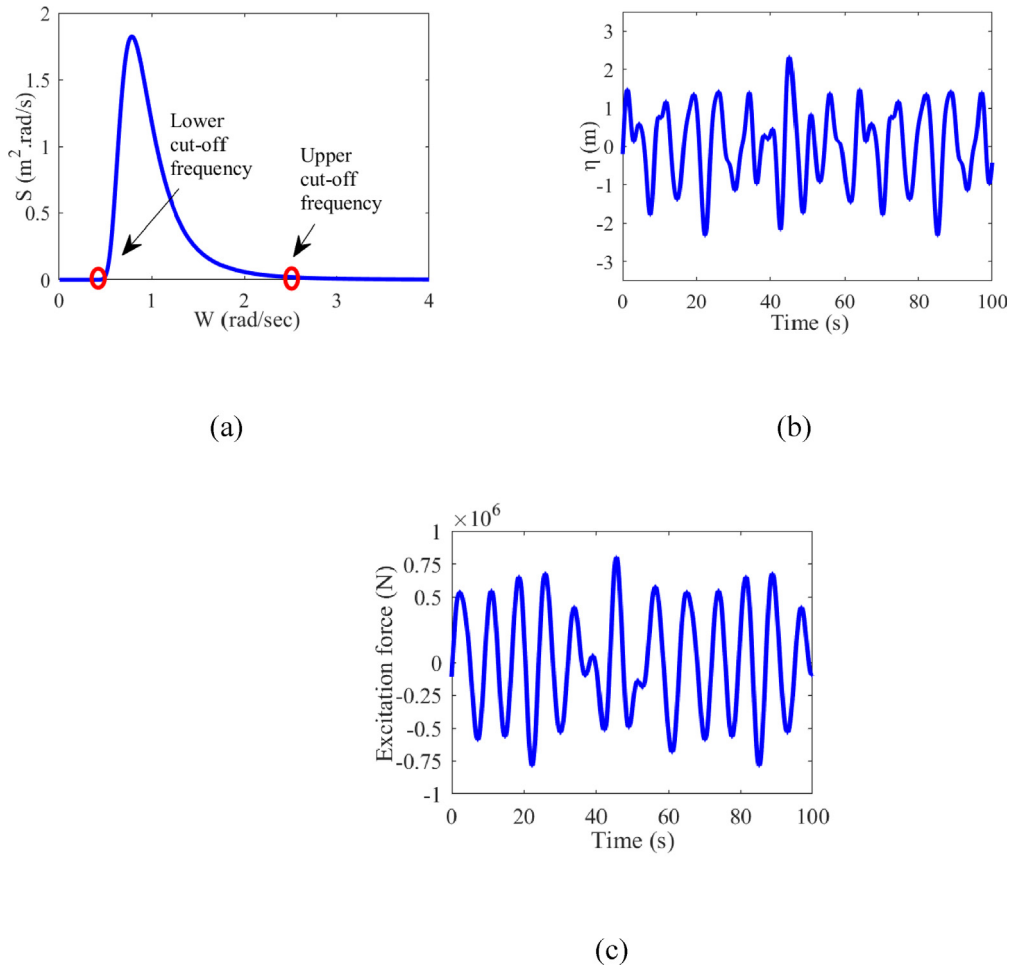


Fig. 5. (a) The Bretschneider spectrum, (b)  $\eta(t)$ , and (c)  $F_e$ .

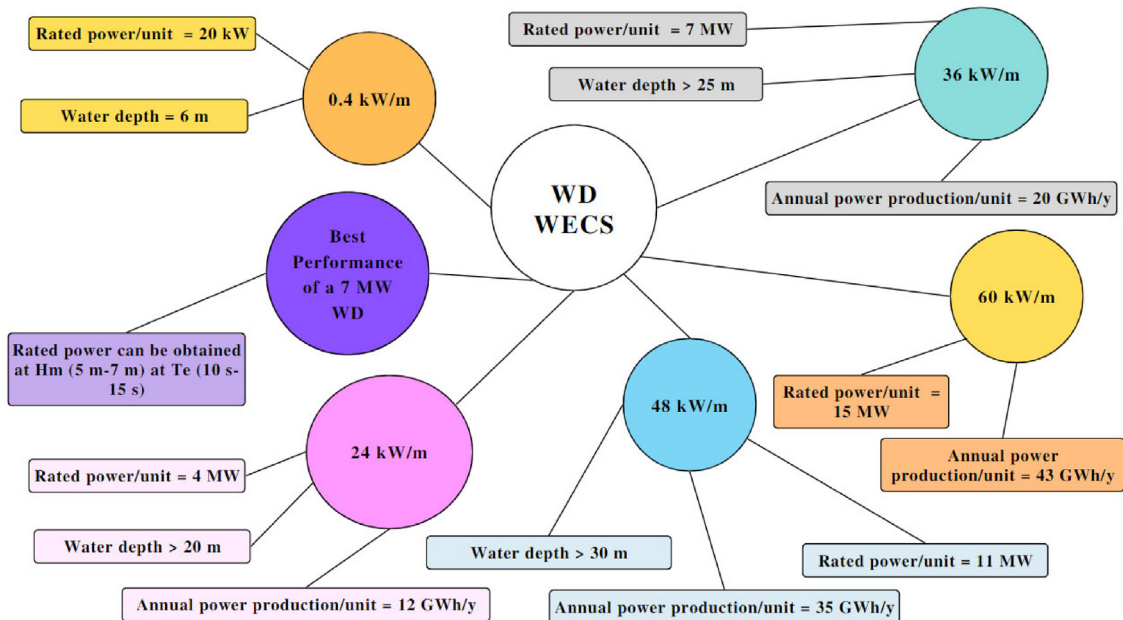


Fig. 6. An overview of WD WECS.

**Table 3**  
WD's Projects and Prototypes.

| Reference Number | Year      | Summary of the project or prototype  |
|------------------|-----------|--|
| [56]             | 1997–2007 | This work gives us several phases towards the development of WD. In 1997, a 1:45 simple WD model was built in a wave tank to obtain primary data about WD. In 1998, a 1:50 floating model was constructed at Danish Maritime Institute. From 1999 to 2001, the WD model was adjusted several times. From 2002 to 2005, a WD prototype scaled at 1:4.5 consisting of 10 turbines was developed in Denmark. This prototype started supplying electrical power to the power grid in 2003. Each generator has a rating of 2.5 kW. Also, this prototype is developed to help deploy a 4 MW WD in the Atlantic or the North Sea by 2007. |
| [59]             | 2006      | Milford Haven Wave Dragon:<br>A 7 MW WD was built 4–5 miles off Milford Haven, offshore Wales. It consists of 18 turbines. Each one of these turbines has a 400 kW generator.  |
| [60]             | 2012      | 1.5 MW Wave Dragon North Sea:<br>This project is a 1.5 MW at the test center DanWEC, Hanstholm. It has been built based on 20,000 test hours of the smaller prototypes. Also, it consists of 8 turbines, and each generator's rating is 185 kW.  |
| [55,61]          | -         | According to the WD company website, preparations are underway for building a 50 MW WD array in Portugal. However, according to the Tethys database, a delay occurred due to the financial crisis in Wave Dragon Ltd company. They are currently looking for investors for research development.   |

Eqs. (18) and (19) are used to obtain  $K_{pw}$  [49]. In these equations,  $k$ ,  $d$ , and  $h$  denote the wave number, the depth, and the seabed depth [50]. As an approximation, in these equations, the force is calculated at the floater's mid-position.  $\eta(t)$  and  $F_e$  are shown in Fig. 5(b) and Fig. 5(c).

$$K_p = \frac{\cosh(k(h-d))}{\cosh kh} \quad (18)$$

$$\omega^2 = gk \tanh(kh) \quad (19)$$

Eqs. (20) – (24) are used to obtain the bearings' frictional force ( $F_{bear}$ ) [51]. In these equations,  $F_{Horizontal}$ ,  $\mu$ ,  $c_M$ ,  $d_{out}$ ,  $c_D$ ,  $u$ , and  $\dot{u}$  are the horizontal force applied on the bearings of the AWS, friction coefficient, inertia coefficient, floater's outer diameter, drag coefficient, horizontal velocity of the wave, and horizontal acceleration of the wave. These values are calculated at mid-position, similar to  $K_p$ . Finally, Eq. (25) is used to get the depth ( $d$ ).

$$F_{bear} = -\mu \cdot \text{sign}(v) |F_H| \quad (20)$$

$$dF_H(z, t) = c_M \rho \frac{\pi}{4} d_{out}^2 \dot{u}(z, t) dz + c_D \rho \frac{1}{2} d_{out} u(z, t) |u(z, t)| dz \quad (21)$$

$$F_H = \int_{z=0}^{z=h_f} dF_H(z, t) \quad (22)$$

$$u = \frac{H\omega}{2} \frac{\cosh(k(h-d))}{\sinh kh} \cos(\omega t) \quad (23)$$

$$\dot{u} = -\frac{H\omega^2}{2} \frac{\cosh(k(h-d))}{\sinh kh} \sin(\omega t) \quad (24)$$

$$d = d_f + h_f - z \quad (25)$$

The generator force ( $F_{gen}$ ) is explained in the next section.

**Table 4**  
WD's Latest Research Work.

| Reference Number | Year | Summary of the research work   |
|------------------|------|--|
| [62]             | 2013 | This work investigates the wave energy deficit in a WD array. An approximate analytical solution describes the diffracted and transmitted waves in the array. This helps in exploring the sensitivity of the wave energy shadow to the level of energy extraction, array configuration, etc. The results suggested that the diffraction spreads part of the waves away from the array shadow region. This diffraction defocuses the wave energy passing through the WD array.  |
| [63]             | 2013 | This work discusses the effect of a wave farm formed of six WDs on the coastal wave climate in the Black Sea. The modeling of this farm is based on the SWAN spectral model. This model's advantage is that it considers the effect of the wave farm presence on the waves. The results show that the waves are affected near the wave farm, but this effect diminishes gradually to the coast. One of the interesting conclusions is that the presence of the wave farm doesn't affect much the nearshore waves. However, the maximum longshore current velocity is more sensitive than $H_s$ in the presence of a wave farm. |
| [64]             | 2014 | This work investigates the sensitivity and the quasi-static analysis of two mooring systems: a single anchor leg mooring (SALM) and a three-legged catenary anchor leg system (CALM). The reference case for the two loads is a 2000 kN horizontal load and a 30 m depth. Also, other parameters were changed around this reference case, such as the depth of water, the horizontal load, and one of the design parameters of the mooring system.   |
| [65]             | 2017 | This work represents the control and modeling of an array of WD WECS that supplies electrical power to the power grid. The system is connected to a medium voltage network. Therefore, each generator has an AC/DC converter merged with a DC/DC boost converter to increase the output voltage. The output is supplied to a DC link connected to a multi-level inverter. This inverter is responsible for controlling the power flow to the grid. Finally, this system was validated experimentally.  |
| [66]             | 2022 | This work compared several renewable energy sources, such as PV, wind, and WD WECS, to a coal-based generating power plant. By using a 7 MW WD instead of a coal power plant, the CO <sub>2</sub> emissions are reduced by 96.9%. Also, acid gases were saved by 99.8%. In addition, the land requirement m <sup>2</sup> /MWh is reduced by 60%. The challenge that the WECSs face is the cost. In this work, the WD WECS cost is 0.09 \$/kWh compared to 0.028 \$/kWh for the coal power plant. Some of these WECS's demerits are the collision with ships and its underwater parts can harm marine life.                     |

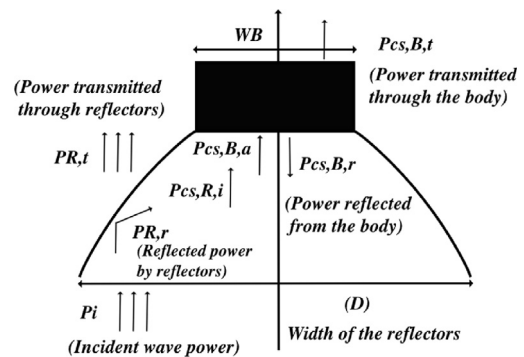


**Fig. 7.** Different types of power in WD WECS.

### 3.4.2. $dq$ frame voltages of the AWS generator

Using Faraday's law, the three-phase output voltages of the AWS linear generator can be represented by Eq. (26) during the positive velocity. In this equation, the three-phase voltages, currents, the resistance, the inductance matrix, and the flux linkage of the stator are denoted by  $v_{abc}$ ,  $i_{abc}$ ,  $R$ ,  $L$ , and  $\psi_{PM-abc}$ , respectively. Eqs. (27) and (28) represent the matrices of both  $L$  and  $\psi_{PM-abc}$ . In these equations,  $L_{ss}$ ,  $M$ ,  $\lambda_{ge}$ , and  $\psi_{PM}$  denote the self-inductance, mutual-inductance, generator pole width, and permanent magnet flux linkage.

$$v_{abc} = -Ri_{abc} + d(-Li_{abc} + \psi_{PM-abc})/dt \quad (26)$$

$$L = \begin{bmatrix} L_{ss} & M & M \\ M & L_{ss} & M \\ M & M & L_{ss} \end{bmatrix} \quad (27)$$

$$\psi_{PM-abc} = \begin{bmatrix} \psi_{PM} \sin(2\pi x/\lambda_{ge}) \\ \psi_{PM} \sin(2\pi x/\lambda_{ge} - 2\pi/3) \\ \psi_{PM} \sin(2\pi x/\lambda_{ge} + 2\pi/3) \end{bmatrix} \quad (28)$$

Also, the three-phase output voltages of the AWS linear generator can be represented by Eq. (29) during the negative velocity when  $v < 0$ .

$$v_{abc} = -Ri_{abc} + d(Li_{abc} + \psi_{PM-abc})/dt \quad (29)$$

A Clarke-Park transformation represented by matrix [K] is utilized to obtain the  $dq$  voltages. [K] is represented by Eq. (30). In this equation, the frames' conversion angle is denoted by  $\theta_t = 2\pi x/\lambda_{ge} - \pi/2$ . The voltages in the  $dq$  frame ( $v_{dq0}$ ) are obtained using Eq. (31).

$$[K] = (2/3) \begin{bmatrix} \cos(\theta_t) & \cos(\theta_t - 2\pi/3) & \cos(\theta_t - 4\pi/3) \\ -\sin(\theta_t) & -\sin(\theta_t - 2\pi/3) & -\sin(\theta_t - 4\pi/3) \\ 1/2 & 1/2 & 1/2 \end{bmatrix} \quad (30)$$

$$v_{dq0} = [K] v_{abc} \quad (31)$$

After applying [K] to  $v_{abc}$  during positive and negative velocities, the direct axis voltage ( $v_d$ ) and quadrature axis voltage ( $v_q$ ) are represented by Eqs. (32) and (33) during the positive velocity. Also,  $v_d$  and  $v_q$  are represented by Eqs. (34) and (35) during the negative

**Table 5**  
PWP's Projects and Prototypes.

| Reference Number | Year      | Summary of the project or prototype   |
|------------------|-----------|---|
| [74]             | 1998–2000 | This work mentions six different experiments on three tank models for the PWP. Two experiments were done on the 80th and 35th scale in 1998. Also, four experiments were done on the 20th scale in 1999 and 2000.   |
| [75]             | 2004–2007 | Between 2004 and 2007, the P1 (the first generation of Pelamis) prototype of 120 m long and a diameter of 3.5 m was developed, tested, and analyzed before installation at the European Marine Energy Centre (EMEC) in Scotland.  |
| [76]             | 2006      | This work provides several tests on a 20th-scale PWP model in a 42 m depth. This model has motorized joints that replicate the control and dynamics of the actual full-scale PWP prototype.   |
| [77]             | 2006      | Aguçadoura Wave Farm Project:<br>In 2006, Enersis, a Portuguese company, developed a 2.25 MW farm of three P1 prototypes on the coast of Peniche in Portugal. Unfortunately, the Babcock & Brown company went bankrupt, ending the project. In 2008, After this incident, the Scottish Power Renewables company took over the project and started developing the second generation of Pelamis "P2." Note that P2 is more efficient than P1. |
| [78]             | 2013–2016 | The Scottish Power Renewables company installed the P2 that ran from 2012 to 2014 in Orkney, Scotland. Then, the Scottish company sold them to EMEC. In 2016, EMEC requested input on the best way to install this system in Lyness, Scotland.  |

velocity [52]. In these equations, induced voltage angular speed and synchronous inductance are denoted by  $\omega_{gen}$  and  $L_s$ , respectively. These values are equal to  $2\pi v/\lambda$  and  $L_{ss} - M$ , respectively.

$$v_d = -Ri_d + \omega_{gen}L_s i_q - L_s(di_d/dt) \quad (32)$$

$$v_q = -Ri_q - \omega_{gen}L_s i_d - L_s(di_q/dt) + \omega_{gen}\psi_{PM} \quad (33)$$

$$v_d = -Ri_d - \omega_{gen}L_s i_q + L_s(di_d/dt) \quad (34)$$

$$v_q = -Ri_q + \omega_{gen}L_s i_d + L_s(di_q/dt) + \omega_{gen}\psi_{PM} \quad (35)$$

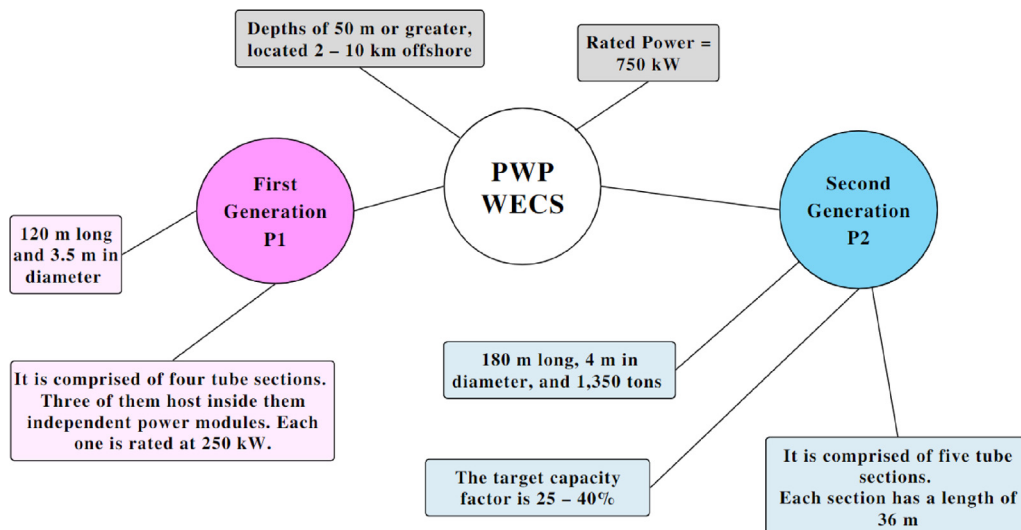


**Fig. 8.** An overview of PWP WECS.

**Table 6**  
PWP's Latest Research Work.

| Reference Number | Year | Summary of the research work   |
|------------------|------|--|
| [79]             | 2018 | This work discusses electrical generation from sea waves using a triboelectric nanogenerator (TENG). The TENG structure is based on the PWP design. Due to the wave's curvature, the TENG can harvest energy from low amplitude sea waves by using polytetrafluoroethylene balls that roll. Also, the snake's segments are connected by springs that allow them to bend easily and produce higher output power. The results show that this generator can be used in water conditions such as in high salinity water. Finally, the TENG proposed has a maximum power density of 3 kW/m <sup>3</sup> .   |
| [80]             | 2018 | This work discusses the stability and bionics of two types of WECSs, cylindrical and elliptical. It provides the essential structural parameters that affect the energy harvest in a three-level sea state. Also, the work discusses the different structural parameters that influence optimum capture efficiency. These parameters were compared to the PWP's design. It is concluded that the energy captured from waves increases when the average wave period is shorter and the average wave height is higher.   |
| [81]             | 2019 | This paper discusses the possibility of combining both wave and wind energies to satisfy electrical needs in the Texas Coast region. The 750 kW PWP was selected for this study. The potential of wave energy was discussed based on the data obtained by the buoys from 2000 to 2012. By combining wind and wave powers, the wave energy variability and installation costs were reduced, and the output power per surface unit increased. One important conclusion is that the wave power output could be much higher for this region if another WECS was selected.  |
| [82]             | 2020 | This work performed a feasibility study of a hybrid renewable energy system that utilizes PV, wind, battery, and PWP. This study discussed the possibility of supplying electrical power to 3000 households in three areas in Iran. The concluded energy cost in Genaveh, Anzali, and Jask using PV, wind, and battery were 0.233, 0.242, and 0.219 \$/kWh, respectively. This system is the best in terms of cost. However, in Anzali, if PWP was included, the cost was reduced to 0.233 \$/kWh. This system is more economical due to the higher potential of waves in the Caspian sea.   |
| [83]             | 2022 | Under the effect of a nonlinear second-order Stokes wave, the dynamic behavior of a P2 was simulated in the AQWA software. This behavior was analyzed in various sea conditions such as $H$ , water depth, angles, and $T_e$ . The results show that as the depth increases, the Pelamis function decreases. Also, the system offers higher operating efficiency during lower wave heights and lower efficiency during long wave periods. Also, the best wave collision angle is when the waves are in the same direction as the WECS. Finally, it was concluded that the performance of the PWP under irregular waves is much better than in the presence of regular waves. |
| [84]             | 2022 | This work analyzed different factors of a WECS like Pelamis to obtain a complete hydraulic model. Using the FORTRAN language, the model was applied to the AQWA software. Also, two simplified models were simulated and compared with the hydraulic model obtained. It was found that the Coulomb torque model was more accurate than the linear damping system model. The Coulomb torque model can simplify the hydraulic model because its motion, energy capture, and torque characteristics are more accurate than the linear damping model. This helps make the utilization of AQWA much easier when simulating the hydraulic model.                                   |

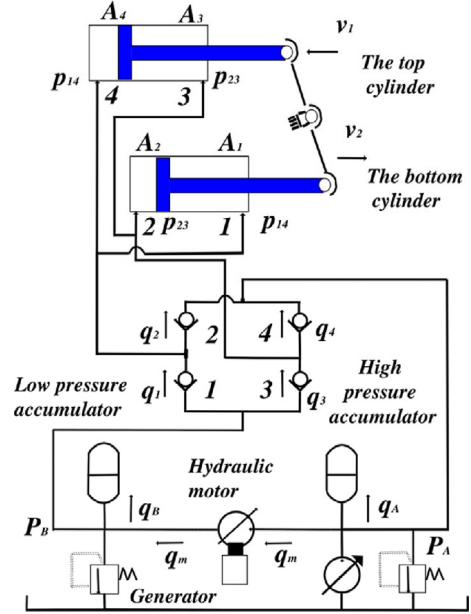


Fig. 9. PWP hydraulic PTO.

$v_d$  and  $v_q$  during both directions can be combined in one compact form represented by Eqs. (36) and (37). In these equations,  $X_s$  represents the synchronous reactance, and its value is equal to  $|\omega_{gen}|L_s$ . Finally, the generator's real power and the force required in the model are represented by Eqs. (38) and (39) [53].

$$v_d = -Ri_d + X_s i_q - L_s (\omega_{gen}/|\omega_{gen}|)(di_d/dt) \quad (36)$$

$$v_q = -Ri_q - X_s i_d - L_s (\omega_{gen}/|\omega_{gen}|)(di_q/dt) + \omega_{gen}\psi_{PM} \quad (37)$$

$$P = 1.5\omega_{gen}i_q\psi_{PM} \quad (38)$$

$$F_{gen} = P/v = (3\omega_{gen}i_q\psi_{PM})/(2v) \quad (39)$$

### 3.4.3. Linear model of the AWS device

In the linearized model,  $F_{bear}$ ,  $F_{drag}$ , and the integral term of  $F_{rad}$  are all neglected. Also, the brakes are applied throughout the whole operation. The linear model can be represented mathematically by Eqs. (40) and (41) [54].

$$v = dx/dt \quad (40)$$

$$F = m_t(dv/dt) + \beta_g v + \beta_{cob} v + k_s x \quad (41)$$

In these equations, the total mass, the generator damping coefficient, the spring constant, and the total force affecting the floater are denoted by  $m_t$ ,  $\beta_g$ ,  $k_s$ , and  $F$ , respectively [39]. In the second equation,  $F_{gen}$  is represented by  $\beta_g v$ . One significant coefficient to notice is the  $\beta_{cob} v$ , which represents the water brake damping force. This force is always operating, limiting the system's actual generating power. Unlike the nonlinear model in which the water brakes operate only when a vertical displacement violation occurs. The spring force  $k_s x$  can be further analyzed into air pressure force ( $F_{Air}$ ), nitrogen cylinder force ( $F_{Nitro}$ ),  $F_{grav}$  and  $F_{HS}$ . This force is represented by Eq. (42).

$$k_s x = F_{Air} + F_{Nitro} + F_{grav} + F_{HS} \quad (42)$$

#### 4. Wave Dragon (WD)

In this section, the most important points of the WD are discussed, in addition to the projects and prototypes involving the WD WECS. Moreover, the latest research regarding WD is discussed in detail. Finally, the mathematical modelling of the WD is presented.

##### 4.1. Introduction to WD

WD is an offshore overtopping WECS in the form of a floating hydroelectric dam. The incoming sea waves are concentrated using reflector wings. These waves are passed up a ramp into a giant floating reservoir. The water is returned to the sea through low-head turbines that generate electrical power. The most important specs of this WECS are illustrated in Fig. 6 [55,56,57,58]. This classification is based on the wave climate (kW/m).

##### 4.2. WD projects and prototypes

There are several projects involving WD WECS and prototypes for testing the WD. A summary of these projects and prototypes is shown in Table 3.

##### 4.3. WD research progress

On Scopus, there are currently 214 research papers about WD. This work performed detailed research on the latest work about WD in the last ten years instead of five years because the research papers focus on assessing the energy source in different locations. This is discussed in a separate section. The most important research works are represented in Table 4.

##### 4.4. WD hydrodynamic model

The WD comprises two main components: the wave reflectors that reflect part of the waves' power to increase the total incident waves towards the main body, in addition to the main body that absorbs as much power as possible from the incident waves. The absorbed power by the main body is represented by Eq. (43) [67]. The different reflected, transmitted, and absorbed powers are illustrated in Fig. 7.

$$P_{cs,B,a} = qR_c g \rho W_B \quad (43)$$

where the main body's absorbed power, the ramp width, the overtopping rate, and the crest freeboard are denoted by  $P_{cs,B,a}$ ,  $W_B$ ,  $q$ , and  $R_c$ , respectively.

$q$  can be obtained by using Eqs. (44) – (46) [68]. In these equations, the non-dimensional overtopping rate, total available power of the waves between the reflectors' cross-section, and the energy flux integrated from the body's draft up to the surface are denoted by  $q_N$ ,  $P_{cs,R,i}$ , and  $P_{dB}$ , respectively. Also, the ratio between  $P_{dB}$  and  $P_{cs,R,i}$  is denoted by  $\lambda_{dB}$ .

$$q = q_N \lambda_{dB} \sqrt{gH_s^3} \quad (44)$$

$$q_N = 0.4e^{-3.2R_c/H_s} \quad (45)$$

$$\lambda_{dB} = P_{dB}/P_{cs,R,i} \quad (46)$$

$P_{cs,R,i}$  can be considered as the total wave power available in the cell of each section. This can be obtained using Eqs. (47) and (48). In these equations, the mean wave energy period, the minus first moment, and the zeroth moment of the wave spectrum are denoted by  $T_e$ ,  $m_{-1}$ , and  $m_0$ , respectively [69].

$$P_{cs,R,i} = \sum_{k=1}^{k=n_{cells}} \frac{\rho g^2}{64\pi} H_{s,k}^2 T_{e,k} \quad (47)$$

$$T_e = m_{-1}/m_0 \quad (48)$$

More in-depth analysis of these equations can be found in [67].

#### 5. Pelamis wave power (PWP)

In this part, the most important points of the PWP are discussed, in addition to the projects and prototypes involving the PWP WECS. Moreover, the latest research regarding PWP is discussed in detail. Finally, the mathematical modelling of the PWP is presented.

##### 5.1. Introduction to PWP

PWP is an offshore floating WECS consisting of a group of semi-submerged cylinders connected using hinged joints [70]. These cylinders move under the effect of the motion of the waves. The PWP WECS contains hydraulic cylinders that resist this motion by pumping high-pressure oil through hydraulic motors using accumulators. These motors drive electrical generators. The most important specs of the two generations of this WECS are illustrated in Fig. 8 [71,72].

##### 5.2. PWP projects and prototypes

There are several projects involving PWP WECS and prototypes for testing the PWP. A summary of these projects and prototypes is shown in Table 5. Several projects weren't mentioned because the Pelamis company announced a layoff in 2012 and went into administration in 2014. This led several companies to end their projects with the Pelamis. Other companies like E.ON pulled out due to the delay in the progress of the wave technology [73].

##### 5.3. PWP research progress

There are currently 1460 research papers on Scopus containing the "Pelmais" keyword. This work performed detailed research on the latest work in the last five years. The most important research works are represented in Table 6.

##### 5.4. PWP hydrodynamic model

The PWP hydraulic cylinder is assumed to be double acting. This means that the cylinder provides oil to the high-pressure accumulator (HPA) regardless of the motion direction. Both lower and upper cylinders transmit force. The PWP section leads to the motion of the upper or lower cylinder of the two cylinders, and the other moves in the opposite direction simultaneously. A schematic diagram for the power take-off (PTO) is illustrated in Fig. 9.

The pressure change in the upper and lower cylinders are expressed by Eqs. (49) and (50), respectively.

$$p_{14} = \frac{\beta_e(q_1 - q_2 - A_4 v_1 + A_1 v_2)}{V_1 + V_4} \quad (49)$$

$$p_{23} = \frac{\beta_e(q_3 - q_4 - A_2 v_2 + A_3 v_1)}{V_3 + V_2} \quad (50)$$

where the volumes of each chamber of the hydraulic cylinders are denoted by  $V_1$ ,  $V_2$ ,  $V_3$ , and  $V_4$ , respectively. Also, the flows of the valves are denoted by  $q_1$ ,  $q_2$ ,  $q_3$ , and  $q_4$ , respectively. Moreover, the action areas of each chamber are denoted by  $A_1$ ,  $A_2$ ,  $A_3$ , and  $A_4$ , respectively. Also, the speeds and the pressures of the chambers

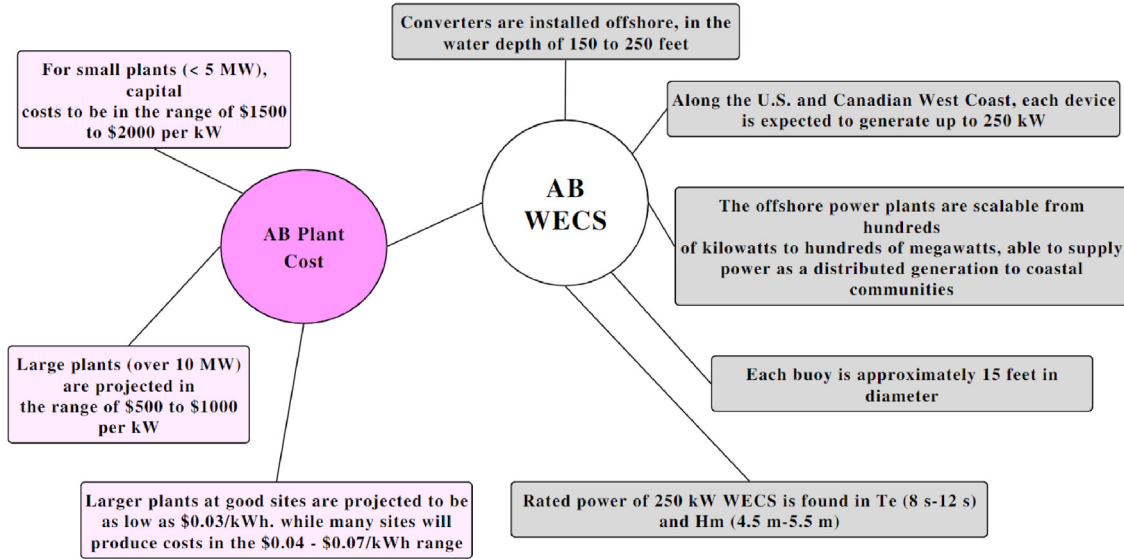


Fig. 10. An overview of AB WECS.

Table 7  
AB's Projects and Prototypes.

| Reference Number | Year | Summary of the project or prototype  |
|------------------|------|--|
| [86]             | 2001 | Makah Bay Offshore Wave Pilot Project: A 1 MW project of four 250 kW ABs provides electrical power to approximately 150 homes near Makah Bay in the USA. This project was canceled in 2009 due to several concerns about project financing and economic feasibility. |
| [87]             | 2007 | A 1:10 scale model of the AB prototype helped analyze the WECS performance in sea testing in Nissum Bredning, Denmark.   |
| [88]             | 2009 | Finavera Renewables, which developed AB, was planning to do several wave projects in Portugal, Canada, South Africa, and the USA. However, in 2009, the company abandoned wave energy and focused on wind energy.  |

are denoted by  $v_1$ ,  $v_2$ ,  $p_{14}$ , and  $p_{23}$ , respectively. Finally, the oil bulk modulus is denoted by  $\beta_e$ . Also, the flow of each one-way valve can be expressed by Eq. (51).

$$q_i = \begin{cases} 0 & : p_1 - p_2 \leq p_3 \\ \frac{K_1(p_1 - p_2 - p_3)\sqrt{p_1 - p_2}}{p_4 - p_3} & : p_3 < p_1 - p_2 \leq p_4 \\ K_2\sqrt{p_1 - p_2} & : p_1 - p_2 > p_4 \end{cases} \quad i = 1, 2, 3, 4 \quad (51)$$

where the inlet pressure, the outlet pressure, the opening pressure, and the maximum opening pressure are denoted by  $p_1$ ,  $p_2$ ,  $p_3$ , and  $p_4$ , respectively. Also, the flow coefficients when the valve doesn't reach the maximum opening and when it reaches the maximum opening are denoted by  $K_1$  and  $K_2$ , respectively.

The flow into HPA ( $q_A$ ), the low-pressure accumulator (LPA) ( $q_B$ ), and the flow into the hydraulic motor ( $q_m$ ) are expressed by Eqs. (52) – (54). In addition, in these equations,  $D_m$  and  $\omega_m$  represent the hydraulic motor displacement and speed, respectively.

$$q_A = q_2 + q_4 - q_m \quad (52)$$

$$q_B = q_m - q_1 - q_3 \quad (53)$$

$$q_m = D_m \omega_m \quad (54)$$

Table 8  
AB's Research Work.

| Reference Number | Year | Summary of the research work   |
|------------------|------|--|
| [85]             | 2003 | This work involves the simulation of the performance of an AB WECS, which includes the development of the numerical model, design optimization, and experimental testing of this WECS. A 1:50 model of AB with different floating systems is evaluated at Aalborg University, Denmark. Also, during the conference, the experimental results were presented. These results include testing under different mooring systems and footprint configurations under survival conditions. In addition, the performance under five sea states was presented. |
| [89]             | 2010 | This work presents the formulation of the equations used to model the vertical motion of the AB WECS. This work includes the equations' numerical solutions that can help predict the output power of this device. The numerical results during irregular and regular waves are presented in the time domain in addition to the experimental results during regular waves.   |
| [90]             | 2019 | This work provides a method for investors to determine the economic feasibility of a floating wave energy farm. This method depends on calculating the Levelized Cost of Energy and the Internal Rate of Return of a wave farm using Geographic Information Systems. This work selected the AB WECS, and the method was applied to the Galician coast in Spain. The results showed that this methodology could help obtain the economic feasibility of different locations, which can help investors.  |

Eqs. (55) and (56) express the liquid volumes of the HPA and LPA accumulators. In these equations, the initial liquid volumes are represented by  $V_{A0}$  and  $V_{B0}$ .

$$V_A = \int_0^t q_A dt + V_{A0} \quad (55)$$

$$V_B = \int_0^t q_B dt + V_{B0} \quad (56)$$

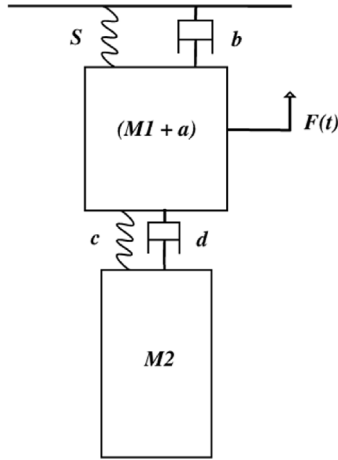


Fig. 11. Modelling of the vertical dynamics of AB.

The pressure of the hydraulic PTO can be expressed by Eq. (57). In this equation, the accumulator pressure, the initial pressure, the accumulator volume, the initial volume, and the adiabatic exponent are denoted by  $P_j$ ,  $P_{j0}$ ,  $V_j$ ,  $V_{j0}$ , and  $\gamma$ , respectively.

$$P_j = P_{j0} \left( \frac{V_{j0}}{V_{j0} - V_j} \right)^\gamma, j = A, B \quad (57)$$

The hydraulic motor driving torque ( $T_m$ ) and the dynamic balance are represented by Eqs. (58) and (59), respectively.

$$T_m = D_m(p_A - p_B) \quad (58)$$

$$\dot{\omega}_m J_m = T_m - T_e - \omega_m B_m - T_c \quad (59)$$

where the hydraulic motor and couplings rotational damping, the generator torque, the hydraulic motor and couplings rotational inertia, and the hydraulic motor Coulomb resistance torque are denoted by  $B_m$ ,  $T_{elec}$ ,  $J_m$ , and  $T_c$ , respectively.

The  $T_{elec}$  is expressed by Eq. (60). In this equation, the generator rotor pole number, the permanent magnet flux linkage, the  $q$ -axis inductance, and the  $d$ -axis inductance are denoted by  $N_p$ ,  $\psi_f$ ,  $L_q$ , and  $L_d$ , respectively.

$$T_{elec} = \frac{3}{2} N_p i_q [(L_d - L_q) i_d + \psi_f] \quad (60)$$

Finally, the buoy kinematic formula can be expressed by Eq. (61).

$$\begin{aligned} & \{M_b + A(\infty)\} \{\ddot{X}(t)\} + \int_{-\infty}^t R(t - \tau) \{\dot{X}(t)\} d\tau + K_{hys} \{X(t)\} \\ & = \{F_{ex}(t)\} + \{F_{pto}(t)\} + \{F_m(t)\} \end{aligned} \quad (61)$$

where the mass matrix, the additional mass matrix, the hysteresis function, hydrostatic recovery stiffness matrix, hydraulic motor force matrix, excitation force matrix, and PTO force matrix are denoted by  $M_b$ ,  $A(\infty)$ ,  $R(t)$ ,  $K_{hys}$ ,  $\{F_m(t)\}$ ,  $\{F_{ex}(t)\}$ , and  $\{F_{pto}(t)\}$ , respectively.

Both  $M_b$  and  $\{F_{ex}(t)\}$  can be obtained using Eqs. (62) and (63), respectively. In these equations, the buoy mass, the buoy gravity coordinates, the buoy moment of inertia around the  $y$ -axis, the buoy force in the surge mode, the buoy force in the heave mode, and the buoy action torque in the pitch mode are denoted by  $m$ ,  $z_G$ ,  $I_5$ ,  $F_{ex}^1$ ,  $F_{ex}^2$ , and  $T_{ex}^3$ , respectively.

$$M_b = \begin{bmatrix} m & 0 & mz_G \\ 0 & m & 0 \\ mz_G & 0 & I_5 \end{bmatrix} \quad (62)$$

$$\{F_{ex}(t)\} = \begin{bmatrix} F_{ex}^1 \\ F_{ex}^2 \\ T_{ex}^3 \end{bmatrix} \quad (63)$$

## 6. AquaBuoy (AB)

In this section, the most important points of the AB are discussed, in addition to the projects and prototypes involving the AB WECS. Moreover, the latest research regarding AB is discussed in detail. Finally, the mathematical modelling of the AB is presented.

### 6.1. Introduction to AB

AB is an offshore floating WECS consisting of a buoy with a vertical tube beneath it. This tube allows seawater to flow through it by opening at both ends. As the water passes, it causes the piston in the middle of the tube to move up and down. This motion causes the extension and compression of a hose pump. Then the pressur-

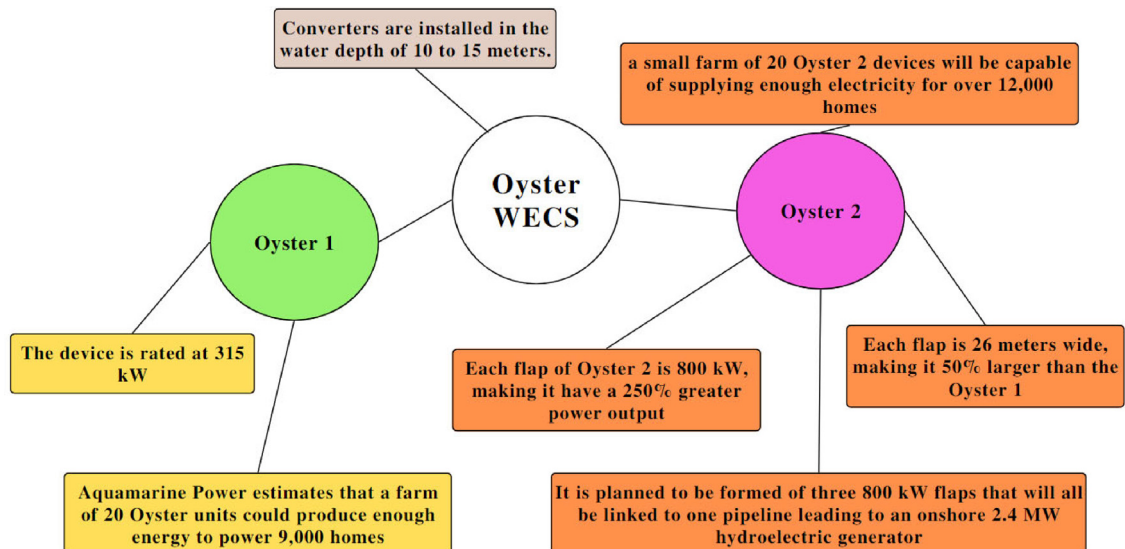


Fig. 12. An overview of Oyster WECS.

**Table 9**  
Oyster's Projects and Prototypes.

| Reference Number | Year | Summary of the project or prototype  |
|------------------|------|--|
| [97]             | 2007 | Several testings were done at Queen's University Belfast containing wave makers capable of generating real and complex sea-states. The majority of these tests were performed using sea-states with a Bretschneider spectrum. The testings were done using 1/40th and 1/20th models. |
| [93]             | 2008 | At the Isleburn shipyard in Nigg bay, the first full-scale Oytester 1 was manufactured.  |
| [98]             | 2009 | The Oyster 1 full-scale WECS was installed at the EMEC. It achieved 6000 h of operation during its two-year lifetime.  |
| [99]             | 2012 | Oyster 2, also known as Oyster 800, was connected to the grid at EMEC's Billia Croo test site until the test was finished in 2015.   |

ized water will be pushed up into the buoy where a turbine exists. This turbine converts the wave motion into electricity. The most important specs of this WECS are illustrated in Fig. 10 [58,85].

### 6.2. AB projects and prototypes

There are several projects involving AB WECS and prototypes for testing the AB. A summary of these projects and prototypes is shown in Table 7.

### 6.3. AB research progress

There are currently 24 research papers on Scopus containing the "AquaBuoy" keyword. Most of these research works focus on assessing the WECS, so the remaining important research works are represented in Table 8.

### 6.4. AB hydrodynamic model

The AB vertical dynamic model is modeled as a two-body system shown in Fig. 11, including the floater connected to a submerged mass. The vertical motion is obtained using D'Alembert's law. This law states that the summation of all forces applied to a body is equal to zero. Eqs. (64) and (65) can represent second-order linear equations of the AB. Also, the fluid friction force ( $F_{ff}$ ) can be calculated using Eq. (66) [91]. In addition, the added mass ( $a_{\infty}$ ) is calculated using Eq. (67).

$$(M_1 + a_{\infty})\ddot{z}_1 + b\dot{z}_1 + S_{hs}z_1 + d_p(\dot{z}_1 - \dot{z}_2) + c(z_1 - z_2) + F_{ff} = F_w(t) \quad (64)$$

$$M_2\ddot{z}_2 = d_p(\dot{z}_1 - \dot{z}_2) + c(z_1 - z_2) \quad (65)$$

$$F_{ff} = A_w C_d \rho \dot{z}_1 |\dot{z}_1| \quad (66)$$

$$a_{\infty} = a(\omega) + \frac{1}{\omega} \int_0^{\infty} h(\tau) \sin(\omega\tau) d\tau \quad (67)$$

where the floater mass, viscous damping, hydrostatic stiffness, the PTO system damping, PTO spring stiffness, the wave excitation force, the water mass in the accelerator tube, the float displacement, the float velocity, the float acceleration, the piston displacement, the piston velocity, the piston acceleration, a measured coefficient (between 1 and 2), floater plan area, and retardation function are denoted by  $M_1$ ,  $b$ ,  $S_{hs}$ ,  $d$ ,  $c$ ,  $F_w(t)$ ,  $M_2$ ,  $z_1$ ,  $\dot{z}_1$ ,  $\ddot{z}_1$ ,  $z_2$ ,  $\dot{z}_2$ ,  $\ddot{z}_2$ ,  $C_d$ ,  $A_w$ , and  $h(\tau)$ , respectively.

For linear damping, the PTO force ( $F_{pto}$ ) and the absorbed power by the PTO ( $P_{abs}$ ) are represented by Eqs. (68) and (69). In addition,

**Table 10**  
Oyster's Research Work.

| Reference Number | Year | Summary of the research work   |
|------------------|------|--|
| [100]            | 2015 | In this work, optimizing an array of oysters was the goal. The array was modeled mathematically, and a semi-analytic method was presented that helped in modeling the hydrodynamics of the device. One of the crucial suggestions is that the optimum width of the flap is 24.6 m instead of 26 m. Several suggestions for optimizing the spaces between WECSs were presented based on this value. In addition, an enhancement in the performance was obtained by staggering the devices. This staggering led to increasing the interactions between them.   |
| [101]            | 2016 | This work discusses a solution for optimizing the layouts of an array of WECSs. The challenge includes the difficulty of analysis, expensive computations, and large computational time, in addition to an increase in these problems with the number of WECSs used in the array. A statistical emulator was utilized to predict the array performance, then an innovative learning strategy that simultaneously explores and focuses on different interest problem regions. Finally, GA is used to obtain the optimal array layout. The advantages of this methodology include being fast and easily scalable according to the array size. The studies were performed on a wave farm consisting of 40 WECSs, specifically, the Oyster.              |
| [102]            | 2016 | In this work, Oyster's hydrodynamics were discussed, which showed some problems in the original design of the rigid flap. Instead of using a rigid flap, six modules of width 24 m will be used. The system interactions of the six modules were analyzed using a mathematical model. The results showed that close units could lead to multiple resonances that can be exploited to harvest more energy. Also, the modules in the center collect more energy than those on the edges. In addition, the power take-off system optimization showed good wave harvest at lower wave periods similar to those obtained by the rigid flap. Also, the modules captured more energy at higher wave periods than the rigid flap due to multiple resonances. |
| [103]            | 2019 | In this work, the efficiency, wave power, and motion response of an Oyster WECS were studied under the effect of irregular waves. Several conclusions were obtained:<br>At any given depth, the energy efficiency and motion response decrease as the wave height increases.<br>As the depth increases, the efficiency of the WECS and the excitation force decrease. This is true until a critical depth value. After which, the WECS performance will remain constant.<br>As the wave frequency increases, the WECS rotation angle and the motion response decrease. This is true until a critical frequency, after which the performance will remain constant.  |
| [104]            | 2020 | This work discusses the environmental impact of Oyster 1 and Oyster 2 at the EMEC in their lifetime. The study includes the ecological consequences, human health, and resource use. Several conclusions were obtained: Oyster 2 has a lower environmental impact than Oyster 1. However, the high infrastructural needs of the WECS technology make it the worst choice compared to other WECSs. Oyster 1 and 2's energy payback period was 42 months and 45 months, respectively. In addition, the carbon footprint for Oyster 1 and 2 was 79 gCO2 eq/kWh and 57 gCO2 eq/kWh, respectively. These values are much worse than most renewable sources but still better than fossil fuels.  |

the nonlinear damping force  $F_{pto}$  can be obtained by combining the linear spring constant with nonlinear Columb damping. This can be done by replacing Eq. (68) with Eq. (70). The excitation force  $F_w(t)$  modeling can be found in [92].

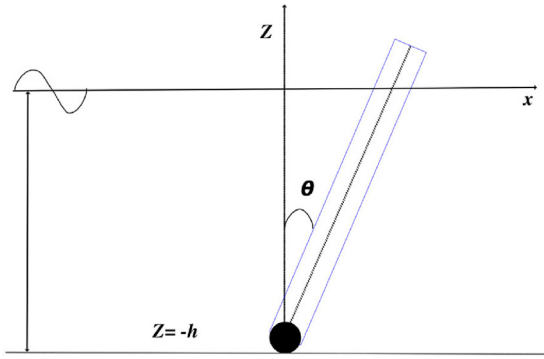


Fig. 13. Oyster vertical cross-section.

$$F_{pto} = d(\dot{z}_1 - \dot{z}_2) + c(z_1 - z_2) \quad (68)$$

$$P_{abs} = F_{pto}(\dot{z}_1 - \dot{z}_2) = d(\dot{z}_1 - \dot{z}_2)^2 + c(z_1 - z_2)(\dot{z}_1 - \dot{z}_2) \quad (69)$$

$$F_{pto} = F_{fric} \text{sign}(\dot{z}_1 - \dot{z}_2) + c(z_1 - z_2) \quad (70)$$

where

$$\text{sign}(x) = \begin{cases} -1 & \text{if } x < 0 \\ 1 & \text{if } x > 0 \\ 0 & \text{if } x = 0 \end{cases} \quad (71)$$

## 7. Oyster

In this section, the most important points of the Oyster are discussed, in addition to the projects and prototypes involving the Oyster WECS. Moreover, the latest research regarding Oysters is discussed in detail. Finally, the mathematical modelling of the Oyster is presented.

### 7.1. Introduction to Oyster

An oyster is formed of a large hinged buoyant flap that moves back and forth by the effect of sea waves. This motion drives two

hydraulic pistons that pressurize freshwater pumped to an onshore hydroelectric turbine. This turbine converts the hydraulic pressure into electrical power. The low-pressure water returns to the device through a different pipeline. The most important specs of this WECS are illustrated in Fig. 12 [93,12,94,95,96].

### 7.2. Oyster projects and prototypes

There are several projects involving Oyster WECS and prototypes for testing the Oyster. A summary of these projects and prototypes is shown in Table 9.

### 7.3. Oyster research progress

There are currently 27 research papers on Scopus containing the ‘‘Oyster Wave Energy Converter’’ keyword. The assessment research works were excluded, and the most important research works in the last ten years are presented in Table 10.

### 7.4. Oyster hydrodynamic model

Oyster mathematical model equations using Laplace equations in the fluid domain can be found in [105] and [106]. The numerical hydrodynamic model of the Oyster can be represented by Eqs. (72) and (73) [98]. Also, the schematic diagram for the Oyster vertical cross-section is shown in Fig. 13.

$$T_w(t) = (I + I_\infty)\ddot{\theta} + \int_{t-\Delta}^t K(t-\tau)\dot{\theta}(\tau)d\tau + k_p \sin(\theta) + B_{nl}\dot{\theta}|\dot{\theta}| + B_{cush}\theta^2\dot{\theta}|\dot{\theta}| + T_{PTO}(t) \quad (72)$$

$$T_w(t) = \int_{t-\Delta_1}^{t+\Delta_2} K_e(t-\tau)\varepsilon(\tau)d\tau \quad (73)$$

where the elevation of the water surface, the surface elevation to the torque impulse response function, the torque of the PTO, the flap rotation, the cushion damping coefficient, the viscous damping coefficient, the pitch stiffness, the radiation impulse function, the added moment of inertia, the moment of inertia of the body, and the incident torque of the wave are denoted by  $\varepsilon$ ,  $K_e$ ,  $T_{PTO}(t)$ ,  $\theta$ ,  $B_{cush}$ ,  $B_{nl}$ ,  $k_p$ ,  $K$ ,  $I_\infty$ ,  $I$ , and  $T_w(t)$ , respectively.

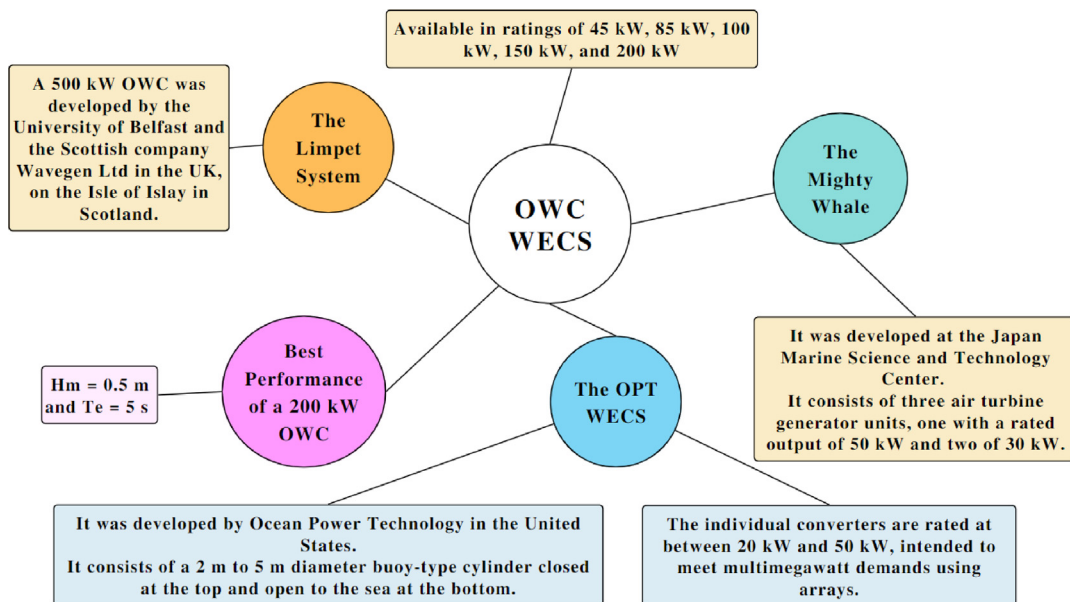


Fig. 14. An overview of OWC WECS.

**Table 11**  
OWC 's Projects and Prototypes.

| Reference Number | Year | Summary of the project or prototype   |
|------------------|------|---|
| [111]            | 1991 | A 75 kW prototype was constructed on Islay island by the Queen's University of Belfast. After the successful experiment, the university and Wavegen planned to build a full-scale OWC.  |
| [112]            | 1996 | A 20 kW OWC prototype was constructed on Dawnshan island in china. After the success of this prototype, a 100 kW OWC was built in the location. This OWC is designed to provide a total rated power of 100 kW at a significant wave height of 1.5 m.  |
| [113]            | 1999 | Pico Power Plant:<br>A 400 kW OWC plant was developed on Pico island in Portugal. This plant was exposed to different problems that ended it. The first unwise decision is avoiding the requirement of unique or expensive resources by having the concrete structure cast on the site. Unfortunately, the contractor's lack of experience led to one of the significant weaknesses of this plant. That's why the replacement of equipment or repairs were always needed. In 2018, a strong sea storm caused a partial collapse of the structure's foundation leading to the project's end.                   |
| [114]            | 2000 | Islay LIMPET:<br>In cooperation with Queen's University Belfast, Wavegen company developed a 500 kW OWC on Islay island. This WECS contained a Wells turbine of 2.6 m diameter. Later, the capacity was downgraded to 250 kW. In 2018, the wave plant was decommissioned, and all the installations were removed except the concrete construction.  |
| [115,116]        | 2011 | Mutriku Breakwater Wave Plant:<br>A 296 kW breakwater oscillating water column (BOWC) was constructed in Mutriku bay in Spain by Ente Vasco de la Energia. This plant is composed of 16 generators, and each one is 18.5 kW. In addition, after nine years of operation, the company announced that BOWC supplied more than 2 GWh to the power grid, which makes it the record holder for the most cumulative operating hours and electricity produced by a WECS. The power plant capacity factor in the years 2014 - 2016 was 0.11. This factor can be enhanced by improving control of the turbine's speed. |
| [117]            | 2014 | Oceanlinx 1 MW Commercial Wave Energy Demonstrator:<br>A 1 MW OWC power plant was intended to be built at Port MacDonnell, South Australia. However, due to transportation complications, the OWC was damaged beyond repair, leading to the end of this project.  |
| [118]            | 2015 | A 500 kW OWC has been installed in South Korea. This OWC is 31.2 m wide and 37 m long.  |

Both  $B_{nl}$  and  $B_{cush}$  are empirical quantities that can be obtained from the tank tests. A more detailed description of the equations can be found in [107].

## 8. Oscillating water column (OWC)

In this section, the most important points of the OWC are discussed, in addition to the projects and prototypes involving the OWC WECS. Moreover, the latest research regarding OWC is discussed in detail. Finally, the mathematical modelling of the OWC is presented.

### 8.1. Introduction to OWC

The OWC is a partially submerged hollow structure. When the sea waves move up and down, this causes the airflow to an air turbine. This turbine rotates, leading to electricity generation. The types of the OWC are illustrated in Fig. 14 [94,108,109,110].

### 8.2. OWC projects and prototypes

There are several projects and prototypes involving OWC WECS. A summary of the important projects and prototypes is shown in Table 11.

### 8.3. OWC research progress

Currently, 827 research papers on Scopus contain the "Oscillating Water Column Wave Energy Converter" keyword. The review of all of these research works will be a complex process. The study will focus on the BOWC. BOWC is similar to an OWC WECS, but the difference is that it acts as a breakwater to protect the shores and, simultaneously, as a WECS [119]. Currently, 48 research papers on Scopus contain the "Breakwater Oscillating Water Column Wave Energy Converter" keyword. The top most cited research works in the last ten years are represented in Table 12.

### 8.4. OWC hydrodynamic model

The fixed-structure OWC linearized equations of motion can be represented using Newton's second law using Eq. (74) [127]. Also, the numerical model can be illustrated using Fig. 15.

$$(M + M_a)\ddot{\eta} + B\dot{\eta} + K_{hr}\eta = f(t) \quad (74)$$

where the water column displacement, speed, and acceleration are denoted by  $\eta$ ,  $\dot{\eta}$ , and  $\ddot{\eta}$ , respectively. Also, the mass of the water column at the still water level ( $M$ ), the added mass ( $M_a$ ), the air damping ( $B$ ), the hydrostatic restoring coefficient ( $K_{hr}$ ), and the total forces acting on the water column ( $f(t)$ ) are represented by Eqs. (75) - (79).

$$M = \rho_w A_1 d \quad (75)$$

$$M_a = \rho_w A_1 \eta \quad (76)$$

$$B = 0.2\sqrt{K(M + M_a)} \quad (77)$$

$$K_{hr} = \rho A_1 g \quad (78)$$

$$f(t) = F_{FK}(t) - F_a(t) - F_{\Delta p}(t) \quad (79)$$

where the chamber area, the wet surface length of the chamber at still water level, Froude- Krylov force, the added mass damping force, and the air force variation are denoted by  $A_1$ ,  $d$ ,  $F_{FK}(t)$ ,  $F_a(t)$ , and  $F_{\Delta p}(t)$ .  $F_a(t)$  can be represented using Eqs. (80) and (81).

$$F_a(t) = M_a \left( \frac{\partial^2 \varphi}{\partial t^2} - \frac{\partial^2 \eta}{\partial t^2} \right) \quad (80)$$

$$\frac{\partial^2 \varphi}{\partial t^2} = \omega^2 \frac{H}{2} \frac{\sinh[k(h-d)]}{\sinh(kh)} \cos(\omega t + \theta_c) \frac{2}{\theta_c} \sin\left(\frac{\theta_c}{2}\right) \quad (81)$$

where the water particle velocity vertical component, the wave height, the chamber angular length, the incident wavelength, the single chamber length, the wave number, the angular wave frequency, the incident wave period, and the water depth are denoted by  $\frac{\partial^2 \varphi}{\partial t^2}$ ,  $H$ ,  $\theta_c$  ( $\theta_c = \frac{2\pi L_c}{L}$ ),  $L$ ,  $L_c$ ,  $k$  ( $k = \frac{2\pi}{L}$ ),  $\omega$  ( $\omega = \frac{2\pi}{T}$ ),  $T$ , and  $h$ .  $F_{FK}(t)$ , the dynamic pressure field ( $P_{wave}(t)$ ), and  $F_{\Delta p}(t)$  can be obtained using Eq. (82) - (84). In Eq. (84),  $\Delta P(t)$  represents the difference in pressure between inside the chamber and the atmospheric pressure.

$$F_{FK}(t) = A_1 P_{wave}(t) \quad (82)$$

$$P_{wave}(t) = \rho g \frac{H}{2} \frac{\cosh[k(h-d)]}{\cosh(kh)} \cos(\omega t + \theta_c) \frac{2}{\theta_c} \sin\left(\frac{\theta_c}{2}\right) \quad (83)$$

**Table 12**  
BOWC 's Research Work.

| Reference Number | Year | Summary of the research work   |
|------------------|------|--|
| [110]            | 2012 | This work provides a methodology to identify the performance of a WECS in a specific location accurately. The methodology is applied to an OWC constructed in Spain at the breakwater of A Guarda. The first step was to characterize the wave climate in the installation site by using energy bins representing wave period, height, and direction. The second step is the computation of the energy resource at the site. The final step includes combining the WECS power matrix with the site's information to determine the WECS's output power.   |
| [120]            | 2013 | This work proposes using asymmetrical (front and rear chambers are not symmetrical) instead of symmetrical chambers in the floating BOWC WECS. The results showed that the motion response and wave transmission in the asymmetrical is as good as the symmetrical configuration. Also, this configuration can help extend the range of frequencies for energy harvest. This system can be helpful in areas that have seasonal variations. Finally, the floating breakwater can be cost-effective as it captures wave power and, at the same time, protect the shorelines  |
| [121]            | 2016 | This work utilizes two large-scale models (1:5 and 1:9) OWCs to investigate the loading and wave reflection. This investigation is under different conditions, such as orifice dimension and water depth. The selection of the orifice dimension that provides minimum wave reflection is the one that will lead to maximum energy harvest. In addition, the forces on the walls and chamber ceiling obtained using formulas are underestimated for the heaviest loading conditions compared to those obtained from the experiments. The experiments showed that setting the relative orifice surface at 0.9% led to a reflection coefficient of 0.5, the minimum value measured, which maximizes the power generated.   |
| [122]            | 2017 | This work investigates the hydrodynamics of two different types of Bent Duct OWCs. One is circular cross-sectional shaped, and the other is rectangular. The numerical analysis was done using a FEM-based frequency domain. In addition, the study was performed experimentally in the Australian Maritime College at frequencies between 0.5 Hz and 1.2 Hz. The numerical analysis and experiments were accurate regarding the volume flux and the capture width. The conclusion is that both the two geometries provided the same results, which means that the geometrical shape has a negligible effect on the captured power. However, the rectangular shape is more viable from constructability and maritime structure integration perspectives.   |
| [123]            | 2019 | This work discusses one of the problems faced during the OWC design: the wave loads' uncertainty. This uncertainty has a critical influence on capital costs. Therefore, an estimation of the forces using a model proposed in this paper is presented. The results were compared with the measurements of a large-scale model in Germany. The results showed that the model fits well with the large-scale model measurements to the factors of $0.8 \pm 0.2$ and $1 \pm 0.2$ for irregular and regular waves, respectively. This model will help in the future constructions of the breakwater OWC WECS with lower uncertainties.  |
| [124]            | 2019 | This work investigated the hydrodynamic performance of an OWC array and a single unit along a straight vertical coast. The OWCs' chambers have different radii, sizes, submergence, and wall thickness. The results showed that the wave energy harvest could be enhanced at certain wave conditions due to the array and constructive coast effects compared to a single unit. In addition, as the radius of the chamber increases, the power capture factor's peaks shift towards the lower frequencies of the waves. Also, the submergence and the OWC wall thickness must be reduced to harvest the highest wave power across large bandwidth. Moreover, the OWCs near the center have the highest peak power capture factor. Finally, the OWCs power harvest can be balanced by using a layout of a non-uniform array.  |
| [125]            | 2019 | In this work, a theoretical model of the OWC was proposed. One of the model's merits is fewer truncating terms in the eigenfunction expansions. Also, the model has no thin-wall restriction and no singularities. Also, this model will be used to investigate the effect of the chamber's radius, submergence, and wall thickness on the wave power harvest. One of the conclusions obtained is that captured power by the WECS increases when the incident sea waves are more perpendicular relative to the breakwater. Another conclusion obtained is that when the ratio of R/h increases, the peak values increase linearly, more resonant and natural frequencies are obtained, bandwidth reduces, and $\eta$ peaks shift toward lower values of wave frequencies. Finally, the smaller the ratio of (R-Ri)/h, the broader and higher the $\eta$ peaks, resulting in more power absorption. |
| [126]            | 2019 | In this work, the hydrodynamics of the OWC were investigated. This is achieved using an analytical method based on linear wave theory and matched eigenfunction expansion. The back-wall draft is increased locally to enhance energy harvest and minimize wave transmission. One of the conclusions is that optimizing the damping of the PTO to obtain maximum power led to enhanced power extraction and wave transmission. However, optimization for minimizing wave transmission led to a reduction in power harvest. That is why the first option is much better. Finally, adopting a two-level practical optimization led to the same wave transmission and power harvest, which is considered the best approach.   |

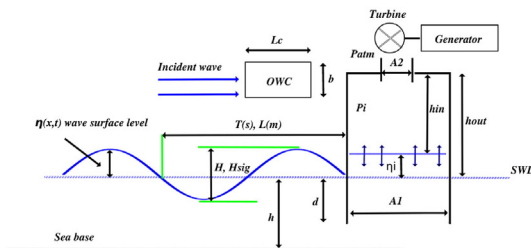


**Fig. 15.** Model of the OWC WECS.

$$F_{\Delta p}(t) = \Delta P(t)A_1 \quad (84)$$

By using the ideal gas equation,  $\Delta P(t)$  can be obtained using Eq. (85).

$$\Delta \dot{P} = \frac{R_g T_k C_d^2 A_2}{A_1 (h_{a0} - \eta)} \sqrt{2 \Delta P \rho_{air}} + \frac{P_c}{h_{a0} - \eta} \quad (85)$$

where the coefficient of discharge, the orifice area, the ideal gas constant, the ambient temperature in Kelvin, the instantaneous chamber pressure, and the height of the chamber top cover to the still water level are denoted by  $C_d$ ,  $A_2$ ,  $R_g$ ,  $T_k$ ,  $P_c$ , and  $h_{a0}$ , respectively.

## 9. Final comparison between the converters investigated in this study

In this section, a summarized comparison between the six converters is provided. This includes the power rating, the suitable depth, the generator type, speed, LCOE, advantages, and disadvantages. This comparison can be summarized in Table 13.

An important note regarding the LCOE, these numbers change based on the location, the wave climate, and the number of units installed [130]. Unfortunately, no study compares the six converters from the LCOE perspective. The values used in the table represent different studies of various locations.

## 10. Wave energy potential

In this section, the wave energy potential in the world and Egypt will be discussed. In addition, the steps required to perform a future feasibility study in Egypt for any nominated location and suggestions for the enhancement of an older study will be provided.

**Table 13**

A Summarized comparison between the six converters.

| Device | Power rating/unit | Suitable depth | Generator type and speed  | LCOE           | Advantages  | Disadvantages  | Reference for LCOE |
|--------|-------------------|----------------|---|----------------|---|--|--------------------|
| AWS    | 15–500 kW         | > 25 m         | LPMSG with variable speed   | Not available  | It is completely submerged, which makes the system less vulnerable to storms. Minimum environmental effect.   | According to the study in [16], the AWS produces a lower amount of energy compared to the other WECSs like OWC, WD, and Pelamis with the same power rating. Hence, a higher power rating AWS is needed to achieve the same annual output energy. | –                  |
| WD     | 20–15000 kW       | > 20 m         | PMSG with variable speed  | 513.17€/MWh    | Great utilization of the installation area. It has a large amount of generated MWh/m <sup>2</sup> compared to the other WECSs. Low maintenance cost, as it can be carried out at sea. Scalable and the most tested WECS technology. | The more water is stored in WD, the heavier it becomes, leading to lower potential energy. In addition to the potential effects on the marine ecosystems.  | [128]              |
| PWP    | 750 kW            | > 50 m         | Induction generator with a fixed speed  | 1710.98€/MWh   | Requires minimal onsite construction and has a low impact on the nearby shoreline.  | The occupation area requirements are very large compared to other WECSs such as the AWS and WD.  | [128]              |
| AB     | 250 kW            | 150–250 feet   | Pelton turbine with a PMSG with a variable speed  | 2627.6€/MWh    | One of the simplest and most promising concepts in WECSs. It can offer energy in remote areas. It has the potential to match seasonal electricity demand with wave power availability.  | It can be a potential problem for ships. It has an expensive structural design that must withstand heavy loading in extreme weather conditions.  | [128]              |
| Oyster | 315 and 800 kW    | 10–15 m        | Induction generator with a variable speed   | 0.35–0.47€/kWh | It has a few moving parts underwater. Its simplicity allows for survivability in extreme weather conditions.  | The high infrastructural needs of the WECS technology make it the worst choice compared to other WECSs. The carbon footprint values are much worse than most renewable sources but still better than fossil fuels.                               | [129]              |
| OWC    | 45–200 kW         | < 20 m         | The Limpet utilizes an induction generator with variable speed. The Pico utilizes a DFIG with a variable speed. | 1.5–2.17€/kWh  | Low maintenance. The BOWC provides two functions, not only acts as a WECS but additionally, it acts as a breakwater to protect the shores.  | Expensive structure. It must withstand harsh stormy conditions.  | [129]              |

10.1. World's wave energy potential

In the literature, several works discuss the global wave energy resource. The wave energy resource strength is measured in kW/m. This represents the annual mean power density which represents how many kW are available in the wave resource per crest width. For example, in [131], the average yearly power density in different locations is provided. The values can reach up to more than 120 kW/m. However, this work lacks several areas, such as the Red Sea (RS) and the Mediterranean Sea (MS). In [132], Seapower wave energy company offers ranges of kW/m for different locations, including RS and MS. According to Seapower, the average wave energy density in MS and RS is between 0 and 15 kW/m.

10.2. Egypt's adoption of renewable energy sources

Egypt has an important strategic position in the world, located in the Arab region and North Africa. In addition, it has long coastlines on RS and MS (nearly 2000 km) [133]. Egypt is still generating electrical power from fossil fuels instead of renewable energy sources, which is one of the biggest concerns of the world bank. If Egypt continues building new fossil fuel-based power plants, the current CO<sub>2</sub> emissions will increase by more than 300% in 2030 [134]. That is why Egypt started new projects that generate electricity from renewable sources, such as wind and solar. Unfortunately, wave energy is not utilized yet in these projects.

10.3. Average power density of waves in RS and MS

Several works studied the average power density of waves in both RS and MS. A summary of the references and power densities is shown in Table 14. A feasibility study is required for the selected WECS location for more precise results.

10.4. Steps for a feasibility study for wave energy in Egypt

In 2010, a feasibility study was conducted for harvesting wave energy in Egypt [135]. This study is divided into five stages. The first four stages can be performed cheaply at educational institutions cooperating with several Egyptian authorities like the Egyptian Meteorological Authority (EMA), the Egyptian Navy, and the New and Renewable Energy Authority (NREA). These phases are explained in brief. In addition, some suggestions are added for the stages to enhance the future actual feasibility study.

- Phase 1: Site Selection

The site is selected based on its wave energy potential. The previous research works can help us choose a suitable location for a wave energy conversion device at the coastlines.

Suggestions:

Previous studies provide values for the annual average power density in MS and RS. For the RS, an assessment of wave energy resources using numerical modeling has been performed [137]. The average wave power in RS obtained in this study can reach up to 4.5 kW/m. For the MS, an assessment based on a 35-year study was conducted [139]. The average energy flux per unit crest (J) for the 1979–2013 period can reach up to 15 kW/m. Moreover, in [140], a study by a group of Italian researchers provided the energy flux values in MS between 2001 and 2010. The values obtained were very close to those obtained in [139].

All these research works can help find a good location for installing our WECS. After selecting some nominated sites in Egypt, wave measurement buoys should be installed in these locations to collect wave data, which can help obtain the wave conditions of a particular site. The wave height ( $H_{m0}$ ), period ( $T_e$ ), and wave direction ( $\theta_m$ ) can be evaluated using Eqs. (86) – (88) [16].

$$H_{m0} = 4(m_0)^{1/2} \tag{86}$$

$$T_e = \frac{m_{-1}}{m_0} \tag{87}$$

$$\theta_m = m_0^{-1} \int_0^{2\pi} \int_0^\infty \theta S(f, \theta) df d\theta \tag{88}$$

where the spectral energy density, frequency, direction, the –1st spectral moment, and 0th spectral moment are denoted by  $S(f, \theta)$ ,  $f$ ,  $\theta$ ,  $m_{-1}$ , and  $m_0$ . Also, the nth spectral moment ( $m_n$ ) can be obtained using Eq. (89).

$$m_n = \int_0^{2\pi} \int_0^\infty f^n S(f, \theta) df d\theta \tag{89}$$

By using these values, J can be calculated using Eq. (90). In this equation, the group celerity ( $C_g$ ) represents the speed at which the wave energy is carried.  $C_g$  can be calculated using Eq. (91) [141].

$$J = \frac{\rho g}{16} H_{m0}^2 C_g \tag{90}$$

$$C_g = \frac{1}{2} \left( 1 + \frac{2kh}{\sinh(2kh)} \right) \left( \frac{gt}{2\pi} \tanh(kh) \right) \tag{91}$$

where  $k$  and  $h$  denote the wave number and the water depth, respectively.

Each of the sea states is assigned to an energy bin. Each energy bin contribution is obtained by multiplying the annual occurrence by the corresponding power. Combining all these states will form a wave energy resource matrix for the selected site in Egypt.

- Phase 2: WECS Selection

The selection of the WECS is very effective in enhancing the wave energy harvest. There are lots of wave energy devices that can be utilized. According to the data obtained from the first stage, suitable WECS can be identified. Also, some factors should be considered when selecting a WECS:

1. The wave spectrum's dominant component should coincide with the most acceptable frequency for the WECS.
2. The WECS should be able to adapt to the sea state variations.
3. The WECS should be able to harvest the other components' energy efficiently.

**Table 14**  
RS and MS power densities.

| Reference Number | Location   | Average power density   |
|------------------|--|---|
| [135]            | MS at Sidi-Barrani                                     | 2–5 kW/m using the Pierson-Moskowitz spectrum.  |
| [136]            | The Eastern Mediterranean Levantine Basin              | 2.5 kW/m in the most energetic offshore area (western coastline of Cyprus).                       |
| [137]            | The eastern coastline of RS                            | 0.89, 1.0, 1.05, and 1.12 kW/m during post-summer, summer, post-winter, and winter, respectively. |
| [138]            | The Southern Mediterranean basin on the Egyptian coast | 6.8 kW/m during winter and 3.35 kW/m during summer, with wave heights between 1 and 4 m.          |

- Phase 3: Computational Modeling and Tank Experiments of the WECSs

The different WECSs' performances must be evaluated numerically (computational modeling) and experimentally (tank experiments) to estimate the annual energy output of these devices.

Suggestions:

The numerical evaluation can be done by combining the power matrix of the WECS with the wave energy resource matrix to obtain how much energy can be produced annually.

- Phase 4: Ecological and Economic Assessments

An economic feasibility study of the WECS should be performed to determine the cost of the generated electrical power [142–145]. It is unlikely that the WECS would be competitive since the existing designs of the WECSs are still developing, and there is currently no WECS that can compete in the market. In addition, an ecological study for the WECS should be performed and ensure that the WECS will fulfill the environmental requirement as a nonpolluting WECS.

- Phase 5: Full-Scale Prototype Deployment

After completing the previous phases, a full-scale prototype for the WECS should be constructed at the site. This will help identify and solve any possible problems that may occur.

## 11. Conclusions

This work summarizes six of the most widely adopted WECSs used heavily in previous research assessments and practical projects. This includes the Archimedes Wave Swing (AWS), the Wave Dragon (WD), Pelamis Wave Power (PWP), Aquabouy (AB), the Oyster, and the Oscillating Water Column (OWC). The work includes the mathematical modeling of these WECSs and the different projects and prototypes involving these WECSs. Moreover, the latest research development in each of these WECSs was presented. Also, the wave energy potential in the world and Egypt was discussed. Finally, the steps required to perform a future feasibility study in Egypt and suggestions for enhancing an older study were provided.

Important key points from the discussion can be presented as follows:

- For the AWS, the WECS is available commercially for wave energy harvest. Each unit has a rating between 15 kW and 500 kW. The units can be combined in an array to form a wave farm. Also, the most significant advantage of this WECS is that it is completely submerged, which means it will not be affected by floating objects.
- WD has units with ratings between 20 kW and up to more than 15 MW. Moreover, WD is a promising WECS as it has been utilized a lot in many assessments of locations worldwide. In many research works, it provided the highest annual energy compared to other WECS. However, the disadvantage of this WECS is that it is a floating WECS, which may be affected by the ships. In addition, the Wave Dragon company is currently suffering from a financial crisis and seeking capital.
- For PWP, there are two generations, P1 and P2. Both of these generations have a rating of 750 kW. Similar to WD, it is one of the most promising WECS. However, the Pelamis company announced a layoff in 2012 and went into administration in 2014. Moreover, PWP is a floating WECS similar to WD, which

means it has the same issue of being affected by the surrounding floating objects. In addition, marine creatures can get trapped in the PWP sections. Also, it can cause visual pollution.

- Also, AB is a floating WECS with a rating of up to 250 kW developed by Finavera Renewables. The company planned to do several wave projects in Portugal, Canada, South Africa, and the USA. However, in 2009, the company abandoned wave energy and focused on wind energy. This is due to the primary concern of the high cost of developing these WECSs.
- There are two types of Oysters 1 and Oyster 2, with a power rating of 315 kW and 800 kW, respectively. The Oyster 1, installed at the EMEC, achieved 6000 h of operation during its two-year lifetime. Also, Oyster 2 was connected to the grid at EMEC's Billia Croo test site until the test was finished in 2015. In [104], the environmental impact of Oyster 1 and Oyster 2 at the EMEC was discussed. Several conclusions were obtained: Oyster 2 has a lower environmental impact than Oyster 1. However, the high infrastructural needs of the WECS technology make it the worst choice compared to other WECSs. Oyster 1 and 2's energy payback period was 42 months and 45 months, respectively. In addition, the carbon footprint for Oyster 1 and 2 was 79 gCO<sub>2</sub> eq/kWh and 57 g CO<sub>2</sub> eq/kWh, respectively. These values are much worse than most renewable sources but still better than fossil fuels.
- The OWC WECS is available at 45 kW and up to 500 kW. The most significant advantage of the OWC is that it can be installed to act as a breakwater and protect the shores from waves while simultaneously converting the incoming waves into electrical power. This will lead to a reduction in the WECS cost. However, the disadvantage is the low annual energy harvest compared to other WECSs, because the waves near the shore are much weaker than those in the deep seas.
- Unfortunately, wave energy conversion technology is not mature enough to compete in the market due to the high cost of WECSs, as these systems should survive in extreme sea conditions. For this reason, several companies have gone bankrupt, and others started working on other renewable sources. However, there is more research on wave energy because wave energy is one of the highest-density sources compared to different renewable energies. Therefore, more development and enhancement of these systems are mandatory for harvesting wave power and making it more economically competitive.
- Moreover, the wave energy potential of both Egypt and the world was presented. Also, the approach for performing a feasibility study in Egypt was introduced. The world's wave energy potential values range from 0 to more than 120 kW/m. Also, Egypt has long coastlines on RS and MS. According to previous works, the average wave energy density in MS and RS is up to 15 kW/m and 4.5 kW/m, respectively. This wave energy amount is not the best compared to other regions worldwide. That is why wave energy may not be economically the best option to generate electricity from RS and MS in Egypt.

## Funding sources

This research did not receive any specific grant from funding agencies in the public, commercial, or not-for-profit sectors.

Data Access Statement.

This study is a reanalysis of existing data, as cited in the references section of this paper. Deposit the final accepted manuscript in BRAD immediately on final publisher acceptance for REF compliance. The data underpinning this publication can be accessed from Brunel University London's data repository, Brunelfigshare, here under a CCBY license: <https://doi.org/10.17633/rd.brunel.5446813.v1>.

## Declaration of Competing Interest

The authors declare that they have no known competing financial interests or personal relationships that could have appeared to influence the work reported in this paper.

## References

- [1] Shen W, Chen X, Qiu J, Hayward JA, Sayeef S, Osman P, et al. A comprehensive review of variable renewable energy leveled cost of electricity. *Renew Sustain Energy Rev* 2020;133:. doi: <https://doi.org/10.1016/j.rser.2020.110301>
- [2] Clemente D, Rosa-Santos P, Taveira-Pinto F. On the potential synergies and applications of wave energy converters: A review. *Renew Sustain Energy Rev* 2021;135:. doi: <https://doi.org/10.1016/j.rser.2020.110162>
- [3] Teixeira-Duarte F, Clemente D, Giannini G, Rosa-Santos P, Taveira-Pinto F. Review on layout optimization strategies of offshore parks for wave energy converters. *Renew Sustain Energy Rev* 2022;163:. doi: <https://doi.org/10.1016/j.rser.2022.112513>
- [4] Si Y, Liu X, Wang T, Feng B, Qian P, Ma Y. State-of-the-art review and future trends of development of tidal current energy converters in China. *Renew Sustain Energy Rev* 2022;167:. doi: <https://doi.org/10.1016/j.rser.2022.112720>
- [5] Rusu L, Onea F. The performance of some state-of-the-art wave energy converters in locations with the worldwide highest wave power. *Renew Sustain Energy Rev* 2017;75:1348–62. doi: <https://doi.org/10.1016/j.rser.2016.11.123>
- [6] Yang B, Wu S, Zhang H, Liu B, Shu H, Shan J, et al. Wave energy converter array layout optimization: a critical and comprehensive overview. *Renew Sustain Energy Rev* 2022;167:. doi: <https://doi.org/10.1016/j.rser.2022.112668>
- [7] Hong Y, Waters R, Boström C, Eriksson M, Engström J, Leijon M. Review on electrical control strategies for wave energy converting systems. *Renew Sustain Energy Rev* 2014;31:329–42. doi: <https://doi.org/10.1016/j.rser.2013.11.053>
- [8] Ilyas A, Kashif SAR, Saqib MA, Asad MM. Wave electrical energy systems: implementation, challenges and environmental issues. *Renew Sustain Energy Rev* 2014;40:260–8. doi: <https://doi.org/10.1016/j.rser.2014.07.085>
- [9] Garcia-Teruel A, Forehand DIM. A review of geometry optimisation of wave energy converters. *Renew Sustain Energy Rev* 2021;139:. doi: <https://doi.org/10.1016/j.rser.2020.110593>
- [10] Bertram DV, Tarighaleslami AH, Walmsley MRW, Atkins MJ, Glasgow GDE. A systematic approach for selecting suitable wave energy converters for potential wave energy farm sites. *Renew Sustain Energy Rev* 2020;132:. doi: <https://doi.org/10.1016/j.rser.2020.110011>
- [11] Penalba M, Ringwood JV. A review of wave-to-wire models for wave energy converters. *Energies* 2016;9. doi: <https://doi.org/10.3390/en9070506>
- [12] Lagoun MS, Benalia A, Benbouzid MEH. Ocean wave converters: State of the art and current status. 2010 IEEE Int Energy Conf Exhib EnergyCon 2010 2010:636–41. 10.1109/ENERGYCON.2010.5771758.
- [13] WAVE ENERGY: Aquabuoys 2.0 Wave Power Generator n.d. <https://inhabitat.com/wave-energy-aquabuoys-20-wave-power-generator/> (accessed August 23, 2022).
- [14] Archimedes Waveswing - AWS Ocean Energy n.d. <https://awsocan.com/archimedes-waveswing/> (accessed July 29, 2022).
- [15] Funding to focus on wave and tidal technologies. *Engineer* 2010;JULY.
- [16] Veigas M, López M, Romillo P, Carballo R, Castro A, Iglesias G. A proposed wave farm on the Galician coast. *Energy Convers Manag* 2015;99:102–11. doi: <https://doi.org/10.1016/j.enconman.2015.04.033>
- [17] Prado MGS, Gardner F. Theoretical analysis of the AWS dynamics during submersion operation. 6th Eur. Wave Tidal Energy Conf., Glasgow, UK: 2005, p. 395–400.
- [18] Cruz JMBP, Sarmento AJNA. Sea state characterisation of the test site of an offshore wave energy plant. *Ocean Eng* 2007;34:763–75. doi: <https://doi.org/10.1016/j.oceaneng.2006.04.004>
- [19] de Sousa Prado MG, Gardner F, Damen M, Polinder H. Modelling and test results of the Archimedes wave swing. *Proc Inst Mech Eng Part A J Power Energy* 2006;220:855–68. doi: <https://doi.org/10.1243/09576509JPE284>
- [20] Chowdhury S De, Nader J. AS preprint arXiv, 2015 undefined. A review of hydrodynamic investigations into arrays of ocean wave energy converters. ArxivOrg n.d.
- [21] Hodgins N, Keysan O, McDonald AS, Mueller MA. Design and testing of a linear generator for wave-energy applications. *IEEE Trans Ind Electron* 2012;59:2094–103. doi: <https://doi.org/10.1109/TIE.2011.2141103>
- [22] Alldritt D, Hopwood D. Renewable energy in Scotland. *Renew Energy Focus* 2010;11:28–33. doi: [https://doi.org/10.1016/S1755-0084\(10\)70064-8](https://doi.org/10.1016/S1755-0084(10)70064-8)
- [23] Patel S. Alstom and SSE renewables prepare for massive offshore wave farm. *Power* 2012;156.
- [24] Wang L, Lin JH, Prokhorov A V., Mokhlis H, Huat CK. Stability analysis of a hybrid wave-energy conversion system with linear permanent-magnet generator driven by Archimedes wave swing and induction generator driven by wells turbine. 2018 IEEE Ind Appl Soc Annu Meet IAS 2018 2018. 10.1109/IAS.2018.8544499.
- [25] Gato LMC, de O. Falcão AF. Aerodynamics of the wells turbine. *Int J Mech Sci* 1988;30:383–95. 10.1016/0020-7403(88)90012-4.
- [26] Nath R, Kankar PK, Gupta VK. Study of archimedes wave swing harvester for Indian Ocean. *Springer Proc Phys* 2019;224:545–56. doi: [https://doi.org/10.1007/978-3-030-19894-7\\_42](https://doi.org/10.1007/978-3-030-19894-7_42)
- [27] Huang J, Yang J, Xie D, Wu D. Optimal sliding mode chaos control of direct-drive wave power converter. *IEEE Access* 2019;7:90922–30. doi: <https://doi.org/10.1109/ACCESS.2019.2925470>
- [28] Hasanien HM. Transient stability augmentation of a wave energy conversion system using a water cycle algorithm-based multiobjective optimal control strategy. *IEEE Trans Ind Informatics* 2019;15:3411–9. doi: <https://doi.org/10.1109/TII.2018.2871098>
- [29] Rasool S, Islam MR, Muttaqi KM, Sutanto D. An Advanced Control Strategy for a Smooth Integration of Linear Generator Based Wave Energy Conversion System with Distribution Power Grids. 2019 IEEE Ind. Appl. Soc. Annu. Meet. IAS 2019, 2019. 10.1109/IAS.2019.8912314.
- [30] González AGE, Verde C, Maya-Ortiz P. FDI study for a wave energy converter by structural analysis. *IFAC-PapersOnLine* 2020;53:13721–6. doi: <https://doi.org/10.1016/j.ifacol.2020.12.876>
- [31] Adaryani MR, Taher SA, Guerrero JM. Model predictive control of direct-drive wave power generation system connected to DC microgrid through DC cable. *Int Trans Electr Energy Syst* 2020;30:1–18. doi: <https://doi.org/10.1002/2050-7038.12484>
- [32] Chuan QIN, Jin M, Chen S, Wang X. Decentralized Power Management of an Islanded Microgrid with AWS-based Wave Energy Converter. *Asia-Pacific Power Energy Eng. Conf. APPEEC*, vol. 2020- Septe, 2020. 10.1109/APPEEC48164.2020.9220380.
- [33] Rasool S, Muttaqi KM, Sutanto D. Modelling of a wave-to-wire system for a wave farm and its response analysis against power quality and grid codes. *Renew Energy* 2020;162:2041–55. doi: <https://doi.org/10.1016/j.renene.2020.10.035>
- [34] Rahman MA, Islam MR, Muttaqi KM, Sutanto D. Modeling and design of a multiport magnetic bus-based novel wind-wave hybrid ocean energy technology. *IEEE Trans Ind Appl* 2021;57:5400–10. doi: <https://doi.org/10.1109/TIA.2021.3087545>
- [35] Wu F, Jing R, Zhang X-P, Wang F, Bao Y. A combined method of improved grey BP neural network and MEEMD-ARIMA for day-ahead wave energy forecast. *IEEE Trans Sustain Energy* 2021;12:2404–12. doi: <https://doi.org/10.1109/TSTE.2021.3096554>
- [36] Rezaei Adaryani M, Taher SA, Guerrero JM. Improved direct model predictive control for variable magnitude variable frequency wave energy converter connected to constant power load. *J Energy Storage* 2021;43. doi: <https://doi.org/10.1016/j.est.2021.103175>
- [37] Turkey RA, Hasanien HM, Alkhuayli A. Dynamic stability improvement of AWS-based wave energy systems using a multiobjective salp swarm algorithm-based optimal control scheme. *IEEE Syst J* 2022;16:79–87. doi: <https://doi.org/10.1109/JSYST.2020.3034277>
- [38] Mirjalili S, Gandomi AH, Mirjalili SZ, Saremi S, Faris H, Mirjalili SM. Salp Swarm Algorithm: a bio-inspired optimizer for engineering design problems. *Adv Eng Softw* 2017;114:163–91. doi: <https://doi.org/10.1016/j.advengsoft.2017.07.002>
- [39] Mahdy A, Hasanien HM, Helmy W, Turkey RA, Abdel Aleem SHE. Transient stability improvement of wave energy conversion systems connected to power grid using anti-windup-coot optimization strategy. *Energy* 2022;245:. doi: <https://doi.org/10.1016/j.energy.2022.123321>
- [40] Naruei I, Keynia F. A new optimization method based on COOT bird natural life model. *Expert Syst Appl* 2021;183:. doi: <https://doi.org/10.1016/j.eswa.2021.115352>
- [41] Mahdy A, Hasanien HM, Hameed WHA, Turkey RA, Aleem SHEA, Ebrahim EA. Nonlinear modeling and real-time simulation of a grid-connected AWS wave energy conversion system. *IEEE Trans Sustain Energy* 2022;13:1744–55. doi: <https://doi.org/10.1109/TSTE.2022.3174176>
- [42] Sharma S, Kapoor R, Dhiman S. A Novel Hybrid Metaheuristic Based on Augmented Grey Wolf Optimizer and Cuckoo Search for Global Optimization. 2021 2nd Int. Conf. Secur. Cyber Comput. Commun., IEEE; 2021, p. 376–81. 10.1109/ICSCCC51823.2021.9478142.
- [43] Mahdy A, Hasanien HM, Turkey RA, Abdel Aleem SHE. Modeling and optimal operation of hybrid wave energy and PV system feeding supercharging stations based on golden jackal optimal control strategy. *Energy* 2023;263:. doi: <https://doi.org/10.1016/j.energy.2022.125932>
- [44] Chopra N, Mohsin AM. Golden jackal optimization: a novel nature-inspired optimizer for engineering applications. *Expert Syst Appl* 2022;198:. doi: <https://doi.org/10.1016/j.eswa.2022.116924>
- [45] Landmann J, Fröhling L, Gieschen R, Buck BH, Heasman K, Scott N, et al. Drag and inertia coefficients of live and surrogate shellfish dropper lines under steady and oscillatory flow. *Ocean Eng* 2021;235:. doi: <https://doi.org/10.1016/j.oceaneng.2021.109377>
- [46] Paul Gieske. Model Predictive Control of a Wave Energy Converter: Archimedes Wave Swing 2007:101.
- [47] McTaggart K. Modelling and Simulation fo Seaways in Deep Water for Simulation of Ship Motions 2003.
- [48] Herber DR, Allison JT. Wave Energy Extraction Maximization in Irregular Ocean Waves Using Pseudospectral Methods. Vol. 3A 39th DES. Autom. Conf., American Society of Mechanical Engineers; 2013. 10.1115/DETC2013-12600.
- [49] Morison JR, Johnson JW, Schaaf SA. The force exerted by surface waves on piles. *J Pet Technol* 1950;2:149–54. doi: <https://doi.org/10.2118/950149-G>

- [50] Agerschou, Hans A. and J. Fifth and first order wave-force coefficients for cylindrical piles. *Asce* 1965.
- [51] Beji S. Applications of Morison's equation to circular cylinders of varying cross-sections and truncated forms. *Ocean Eng* 2019;187:.. doi: <https://doi.org/10.1016/j.oceaneng.2019.106156>106156.
- [52] Feng Wu, Zhang XP, Ping Ju, Sterling MJH. Optimal control for AWS-based wave energy conversion system. *IEEE Trans Power Syst* 2009;24:1747–55. doi: <https://doi.org/10.1109/TPWRS.2009.2030294>.
- [53] Hasanien HM. Gravitational search algorithm-based optimal control of archimedes wave swing-based wave energy conversion system supplying a DC microgrid under uncertain dynamics. *IET Renew Power Gener* 2017;11:763–70. doi: <https://doi.org/10.1049/iet-rpg.2016.0677>.
- [54] Wu F, Zhang XP, Ju P, Sterling MJH. Modeling and control of AWS-based wave energy conversion system integrated into power grid. *IEEE Trans Power Syst* 2008;23:1196–204. doi: <https://doi.org/10.1109/TPWRS.2008.922530>.
- [55] Specifications n.d. <http://wavedragon.net/specifications/> (accessed August 8, 2022).
- [56] Kofoed JP, Frigaard P, Friis-Madsen E, Sørensen HC. Prototype testing of the wave energy converter wave dragon. *Renew Energy* 2006;31:181–9. doi: <https://doi.org/10.1016/j.renene.2005.09.005>.
- [57] Esteban MD, López-Gutiérrez JS, Negro V, Laviña M, Muñoz-Sánchez P. A new classification of wave energy converters used for selection of devices. *J Coast Res* 2018;85:1286–90. doi: <https://doi.org/10.2112/SI85-258.1>.
- [58] Silva D, Rusu E, Soares CG. Evaluation of various technologies for wave energy conversion in the portuguese nearshore. *Energies* 2013;6:1344–64. doi: <https://doi.org/10.3390/en6031344>.
- [59] Vining JC. Worlds Largest Wave Energy Project 2007 in Wales. *Proc POWER-GEN 2006 Eur Conf* 2007.
- [60] Friis-Madsen E, Sørensen HCC, Parmeggiani S. The development of a 1.5 MW wave dragon north sea demonstrator.. 4th Int Conf Ocean Energy 2012:1–5.
- [61] Wave Dragon Pre-Commercial Demonstration Project | Tethys n.d. <https://tethys.pnnl.gov/project-sites/wave-dragon-pre-commercial-demonstration-project> (accessed August 8, 2022).
- [62] Monk K, Zou Q, Conley D. An approximate solution for the wave energy shadow in the lee of an array of overtopping type wave energy converters. *Coast Eng* 2013;73:115–32. doi: <https://doi.org/10.1016/j.coastaleng.2012.10.004>.
- [63] Diaconu S, Rusu E. The environmental impact of a wave dragon array operating in the Black Sea. *Sci World J* 2013. doi: <https://doi.org/10.1155/2013/498013>.
- [64] Pecher A, Foglia A, Kofoed JP. Comparison and sensitivity investigations of a CALM and SALM type mooring system for wave energy converters. *J Mar Sci Eng* 2014;2:93–122. doi: <https://doi.org/10.3390/jmse2010093>.
- [65] Muller N, Kouro S, Malinowski M, Rojas CA, Jasinski M, Estay G. Medium-voltage power converter interface for multigenerator marine energy conversion systems. *IEEE Trans Ind Electron* 2017;64:1061–70. doi: <https://doi.org/10.1109/TIE.2016.2615276>.
- [66] Banerjee S. Theoretical design for ascertaining sustainability of energy systems with special reference to the competing renewable energy schemes. *Resour Environ Sustain* 2022;7. doi: <https://doi.org/10.1016/j.resenv.2022.100048>.
- [67] Kofoed JP. Wave Overtopping of Marine Structures: utilization of wave energy. *Uniw Śląski* 2002:343–54. 10.2//QUERY.MIN.JS.
- [68] Beels C, Troch P, De Visch K, Kofoed JP, De Backer G. Application of the time-dependent mild-slope equations for the simulation of wake effects in the lee of a farm of Wave Dragon wave energy converters. *Renew Energy* 2010;35:1644–61. doi: <https://doi.org/10.1016/j.renene.2009.12.001>.
- [69] Carballo R, Sánchez M, Ramos V, Taveira-Pinto F, Iglesias G. A high resolution geospatial database for wave energy exploitation. *Energy* 2014;68:572–83. doi: <https://doi.org/10.1016/j.energy.2014.02.093>.
- [70] Henderson R. Design, simulation, and testing of a novel hydraulic power take-off system for the Pelamis wave energy converter. *Renew Energy* 2006;31:271–83. doi: <https://doi.org/10.1016/j.renene.2005.08.021>.
- [71] Polinder H, Scuotto M. Wave energy converters and their impact on power systems. 2005 Int Conf Futur Power Syst 2005;2005. 10.1109/FPS.2005.204210.
- [72] Yemm R, Pizer D, Retzler C, Henderson R. Pelamis: experience from concept to connection. *Philos Trans R Soc A Math Phys Eng Sci* 2012;370:365–80. doi: <https://doi.org/10.1098/RSTA.2011.0312>.
- [73] E.ON Pulls Out of Pelamis Wave Energy Project (UK) - Offshore Energy n.d.
- [74] Carcas M, Yemm RW, Henderson RM, Taylor AE. The opd pelamis wec: current status and onward programme. *ResearchgateNet* 2003;24:21–8. doi: <https://doi.org/10.1080/01430750.2003.9674899>.
- [75] Gobato R, Gobato A, Fedrigo DFG. Study Pelamis system to capture energy of ocean wave 2015:1–31.
- [76] Retzler C. Measurements of the slow drift dynamics of a model Pelamis wave energy converter. *Renew Energy* 2006;31:257–69. doi: <https://doi.org/10.1016/j.renene.2005.08.025>.
- [77] Gobato R, Gobato A, Fedrigo DFG. Harnessing the energy of ocean surface waves by Pelamis System. *Parana J Sci Educ* 2016;2:1–15.
- [78] Pelamis Wave Power - Furnace Compare n.d. <https://www.furnacecompare.com/blog/energy-efficiency/pelamis-wave-power/> (accessed August 10, 2022).
- [79] Zhang SL, Xu M, Zhang C, Wang Y-C, Zou H, He X, et al. Rationally designed sea snake structure based triboelectric nanogenerators for effectively and efficiently harvesting ocean wave energy with minimized water screening effect. *Nano Energy* 2018;48:421–9. doi: <https://doi.org/10.1016/j.nanoen.2018.03.062>.
- [80] Dong J, Gao J, Zheng P, Zhang Y. Numerical simulation and structural optimization based on an elliptical and cylindrical raft wave energy conversion device. *J Renew Sustain Energy* 2018;10. doi: <https://doi.org/10.1063/1.5042269>.
- [81] Haces-Fernandez F, Li H, Jin K. Investigation into the possibility of extracting wave energy from the texas coast. *Int J Energy a Clean Environ* 2019;20:23–41. doi: <https://doi.org/10.1615/InterJEnergyCleanEnv.2018019929>.
- [82] Jahangir MH, Shahsavari A, Vaziri Rad MA. Feasibility study of a zero emission PV/Wind turbine/Wave energy converter hybrid system for stand-alone power supply: a case study. *J Clean Prod* 2020;262:.. doi: <https://doi.org/10.1016/j.jclepro.2020.121250>121250.
- [83] Ghaneei H, Mahmoudi M. Simulation, optimization and economic assessment of pelamis wave energy converter. *J Ocean Technol* 2022;17:76–98.
- [84] Huang Q, Wang P, Liu Y, Li B. Modeling and Simulation of Hydraulic Power Take-Off Based on AQWA. *Energies* 2022, Vol 15, Page 3918 2022;15:3918. 10.3390/EN15113918.
- [85] Weinstein A, Fredrikson G, Claeson L, Forsberg J, Parks MJ, Nielsen K, et al. AquaBuOY—the offshore wave energy converter numerical modeling and optimization. *Ocean*. 2003 *Celebr. Past... Teaming Towar. Futur.*, vol. 4, 2003, p. 1988–95. 10.1109/OCEANS.2003.178203.
- [86] Makah Bay Offshore Wave Pilot Project | Tethys n.d. <https://tethys.pnnl.gov/project-sites/makah-bay-offshore-wave-pilot-project> (accessed August 16, 2022).
- [87] Vicinanza D, Margheritini L, Frigaard P. AquabuoY Wave Energy Converter: Real Sea Testing at Nissum Bredning (Denmark). *Uniw Śląski* 2007:343–54. 10.2//QUERY.MIN.JS.
- [88] Bald J, Campo A, Franco J, Galparsoro I, González M, Liria P, et al. Protocol to develop an environmental impact study of wave energy converters. *Rev Investig Mar* 2010;17:62–138.
- [89] Wachter A. Mathematical and numerical modeling of the AquaBuOY wave energy converter. *Math Case Stud* 2010;2:16–33.
- [90] Castro-Santos L, Filgueira-Vizoso A, Piegari L. Calculation of the levelized cost of energy and the internal rate of return using GIS: the case study of a floating wave energy farm. *ICCEP 2019–7th Int. Conf Clean Electr Power Renew Energy Resour Impact* 2019:674–9. doi: <https://doi.org/10.1109/ICCEP.2019.8890168>.
- [91] Newman JN. *Marine Hydrodynamics*. The MIT Press; 1977. 10.7551/mitpress/4443.001.0001.
- [92] Newman JN. The exciting forces on fixed bodies in waves. *J Sh Res* 1962;6:10–7. doi: <https://doi.org/10.5957/jsr.1962.6.4.10>.
- [93] Henry A, Doherty K, Cameron L, Doherty R, Whittaker T. *Advances in the design of the oyster wave energy converter*. RINA, R Inst Nav Archit - Mar Renew Offshore Wind Energy - Pap 2010:119–28.
- [94] Poullikkas A. Technology prospects of wave power systems. *Electron J Energy Environ* 2014;47–69. doi: <https://doi.org/10.7770/ejee-V2N1-art662>.
- [95] Zanol AT, Onea F, Rusu E. Evaluation of the coastal influence of a generic wave farm operating in the romanian nearshore. *J Environ Prot Ecol* 2014;15:597–605.
- [96] Aquamarine Power's Oyster 2: Can it help wave energy go commercial? | ZDNet n.d. <https://www.zdnet.com/article/aquamarine-powers-oyster-2-can-it-help-wave-energy-go-commercial/> (accessed August 17, 2022).
- [97] Whittaker T, Collier D, Folley M, Osterried M, Henry A. The development of Oyster - A shallow water surging wave energy converter . 7th Eur Wave Tidal Energy Conf 2007:11–4.
- [98] O'Boyle L, Doherty K, van 't Hoff J, Skelton J. The Value of Full Scale Prototype Data - Testing Oyster 800 at EMEC , Orkney. *Proc 11th Eur Wave Tidal Energy Conf* 2015:1–10.
- [99] Aquamarine Power : EMEC: European Marine Energy Centre n.d. <https://www.emec.org.uk/about-us/wave-clients/aquamarine-power/> (accessed August 17, 2022).
- [100] Noad IF, Porter R. Optimisation of arrays of flap-type oscillating wave surge converters. *Appl Ocean Res* 2015;50:237–53. doi: <https://doi.org/10.1016/j.apor.2015.01.020>.
- [101] Sarkar D, Contal E, Vayatis N, Dias F. Prediction and optimization of wave energy converter arrays using a machine learning approach. *Renew Energy* 2016;97:504–17. doi: <https://doi.org/10.1016/j.renene.2016.05.083>.
- [102] Sarkar D, Doherty K, Dias F. The modular concept of the Oscillating Wave Surge Converter. *Renew Energy* 2016;85:484–97. doi: <https://doi.org/10.1016/j.renene.2015.06.012>.
- [103] Yuan Z, Zhang L, Zhou B, Jin P, Zheng X. Analysis of the hydrodynamic performance of an oyster wave energy converter using star-CCM+. *J Mar Sci Appl* 2019;18:153–9. doi: <https://doi.org/10.1177/0957650919867191>.
- [104] Karan H, Thomson RC, Harrison GP. Full life cycle assessment of two surge wave energy converters. *Proc Inst Mech Eng Part A J Power Energy* 2020;234:548–61. doi: <https://doi.org/10.1177/0957650919867191>.
- [105] Koley S, Trivedi K. Mathematical modeling of Oyster wave energy converter device, 2020, p. 130014. 10.1063/5.0025237.
- [106] Renzi E, Dias F. Hydrodynamics of the oscillating wave surge converter in the open ocean. *Eur J Mech - B/Fluids* 2013;41:1–10. doi: <https://doi.org/10.1016/j.euromechflu.2013.01.007>.
- [107] van 't Hoff. *Hydrodynamic Modelling of the Oscillating Wave Surge Converter*. Queen's Univ Belfast 2009.

- [108] Falcão AFO, Gato LMC. Air turbines.. *Compr Renew Energy* 2012;8:111–49. doi: <https://doi.org/10.1016/B978-0-08-087872-0.00805-2>.
- [109] Bricker JD, Esteban M, Takagi H, Roeber V. Economic feasibility of tidal stream and wave power in post-Fukushima Japan. *Renew Energy* 2017;114:32–45. doi: <https://doi.org/10.1016/j.renene.2016.06.049>.
- [110] Carballo R, Iglesias G. A methodology to determine the power performance of wave energy converters at a particular coastal location. *Energy Convers Manag* 2012;61:8–18. doi: <https://doi.org/10.1016/j.enconman.2012.03.008>.
- [111] Østergaard I, Iversen S, Energicenter Danmark, European Wave Energy Conference (4 : 2000 : Aalborg). The design, construction and operation of the LIMPET wave energy converter (Islay, Scotland)[Land Installed Powered Marine Energy Transformer] 2001.
- [112] Zhang D, Li W, Lin Y. Wave energy in China: current status and perspectives. *Renew Energy* 2009;34:2089–92. doi: <https://doi.org/10.1016/j.renene.2009.03.014>.
- [113] Falcão AFO, Sarmento AJNA, Gato LMC, Brito-Melo A. The Pico OWC wave power plant: Its lifetime from conception to closure 1986–2018. *Appl Ocean Res* 2020;98:. doi: <https://doi.org/10.1016/j.apor.2020.102104>.
- [114] Boake CB, Whittaker TJT, Folley M, Ellen H. Overview And Initial Operational Experience of the LIMPET Wave Energy Plant 2002.
- [115] Ibarra-Berastegi G, Sáenz J, Ulazia A, Serras P, Esnaola G, Garcia-Soto C. Electricity production, capacity factor, and plant efficiency index at the Mutriku wave farm (2014–2016). *Ocean Eng* 2018;147:20–9. doi: <https://doi.org/10.1016/j.oceaneng.2017.10.018>.
- [116] Mutriku Wave Plant Hits 2GWh Mark - Offshore Energy n.d. <https://www.offshore-energy.biz/mutriku-wave-plant-hits-2gwh-mark/> (accessed August 22, 2022).
- [117] Oceanlinx 1MW Commercial Wave Energy Demonstrator - Australian Renewable Energy Agency (ARENA) n.d. <https://arena.gov.au/projects/oceanlinx-1mw-commercial-wave-energy-demonstrator/> (accessed August 22, 2022).
- [118] Falcão AFO, Henriques JCC. Oscillating-water-column wave energy converters and air turbines: a review. *Renew Energy* 2016;85:1391–424. doi: <https://doi.org/10.1016/j.renene.2015.07.086>.
- [119] Tanimoto K, Takahashi S. Design and construction of caisson breakwaters – the Japanese experience. *Coast Eng* 1994;22:57–77. doi: [https://doi.org/10.1016/0378-3839\(94\)90048-5](https://doi.org/10.1016/0378-3839(94)90048-5).
- [120] He F, Huang Z, Law AWK. An experimental study of a floating breakwater with asymmetric pneumatic chambers for wave energy extraction. *Appl Energy* 2013;106:222–31. doi: <https://doi.org/10.1016/j.apenergy.2013.01.013>.
- [121] Viviano A, Naty S, Foti E, Bruce T, Allsop W, Vicinanza D. Large-scale experiments on the behaviour of a generalised Oscillating Water Column under random waves. *Renew Energy* 2016;99:875–87. doi: <https://doi.org/10.1016/j.renene.2016.07.067>.
- [122] Howe D, Nader JR. OWC WEC integrated within a breakwater versus isolated: experimental and numerical theoretical study. *Int J Mar Energy* 2017;20:165–82. doi: <https://doi.org/10.1016/j.ijome.2017.07.008>.
- [123] Pawitan KA, Dimakopoulos AS, Vicinanza D, Allsop W, Bruce T. A loading model for an OWC caisson based upon large-scale measurements. *Coast Eng* 2019;145:1–20. doi: <https://doi.org/10.1016/j.coastaleng.2018.12.004>.
- [124] Zheng S, Antonini A, Zhang Y, Greaves D, Miles J, Iglesias G. Wave power extraction from multiple oscillating water columns along a straight coast. *J Fluid Mech* 2019;878:445–80. doi: <https://doi.org/10.1017/jfm.2019.656>.
- [125] Zheng S, Zhang Y, Iglesias G. Coast/breakwater-integrated OWC: a theoretical model. *Mar Struct* 2019;66:121–35. doi: <https://doi.org/10.1016/j.marstruc.2019.04.001>.
- [126] He F, Zhang H, Zhao J, Zheng S, Iglesias G. Hydrodynamic performance of a pile-supported OWC breakwater: an analytical study. *Appl Ocean Res* 2019;88:326–40. doi: <https://doi.org/10.1016/j.apor.2019.03.022>.
- [127] Shalby M, Walker P, Dorrell DG. Modelling of the multi-chamber oscillating water column in regular waves at model scale. *Energy Procedia* 2017;136:316–22. doi: <https://doi.org/10.1016/j.egypro.2017.10.261>.
- [128] Castro-Santos L, Bento A, Guedes SC. The economic feasibility of floating offshore wave energy farms in the north of Spain. *Energies* 2020;13:806. doi: <https://doi.org/10.3390/en13040806>.
- [129] Sergent P, Baudry V, De BA, Michard B, Dugor J. Numerical assessment of onshore wave energy in France: wave energy conversion and cost. *J Mar Sci Eng* 2020;8:947. doi: <https://doi.org/10.3390/jmse8110947>.
- [130] Guo C, Sheng W, De Silva DG, Aggidis G. A review of the levelized cost of wave energy based on a techno-economic model. *Energies* 2023;16:1–30. doi: <https://doi.org/10.3390/en16052144>.
- [131] Folley M. The Wave Energy Resource 2017:43–79. doi: [https://doi.org/10.1007/978-3-319-39889-1\\_3](https://doi.org/10.1007/978-3-319-39889-1_3).
- [132] LCOE – Seapower n.d. <http://www.seapower.ie/cost-of-energy/> (accessed August 30, 2022).
- [133] Amin I, Ali MEA, Bayoumi S, Oterkus S, Shawky H, Oterkus E. Conceptual Design and Numerical Analysis of a Novel Floating Desalination Plant Powered by Marine Renewable Energy for Egypt. *J Mar Sci Eng* 2020, Vol 8, Page 95 2020;8:95. 10.3390/JMSE8020095.
- [134] Abdallah L, El-Shennawy T. Evaluation of CO2 emission from Egypt's future power plants. *Euro-Mediterranean J Environ Integr* 2020.1–8;.53:5. doi: <https://doi.org/10.1007/S41207-020-00184-W>.
- [135] Bayoumi AS, El-Gamal HA. Research plan for harnessing wave energy in Egypt IEEE 17Th. *Int. Conf. Ind. Eng. Eng. Manag. IEEE* 2010:108–10. doi: <https://doi.org/10.1109/ICIEEM.2010.5646628>.
- [136] Zodiatis G, Galanis G, Nikolaidis A, Kalogeri C, Hayes D, Georgiou GC, et al. Wave energy potential in the Eastern Mediterranean Levantine Basin. an integrated 10-year study. *Renew. Energy* 2014;69:311–23. doi: <https://doi.org/10.1016/j.renene.2014.03.051>.
- [137] Aboobacker VM, Shanas PR, Alsaafani MA, Albarakati AMA. Wave energy resource assessment for Red Sea. *Renew Energy* 2017;114:46–58. doi: <https://doi.org/10.1016/j.renene.2016.09.073>.
- [138] Shehata AS, Xiao Q, El-Shaib M, Sharara A, Alexander D. Comparative analysis of different wave turbine designs based on conditions relevant to northern coast of Egypt. *Energy* 2017;120:450–67. doi: <https://doi.org/10.1016/j.energy.2016.11.091>.
- [139] Besio G, Mentaschi L, Mazzino A. Wave energy resource assessment in the Mediterranean Sea on the basis of a 35-year hindcast. *Energy* 2016;94:50–63. doi: <https://doi.org/10.1016/j.energy.2015.10.044>.
- [140] Liberti L, Carillo A, Sannino G. Wave energy resource assessment in the Mediterranean, the Italian perspective. *Renew Energy* 2013;50:938–49. doi: <https://doi.org/10.1016/j.renene.2012.08.023>.
- [141] Dean RG, Dalrymple RA. *Water Wave Mechanics for Engineers and Scientists* 1991;2. 10.1142/1232.
- [142] Shields MA, Dillon LJ, Woolf DK, Ford AT. Strategic priorities for assessing ecological impacts of marine renewable energy devices in the Pentland Firth (Scotland, UK). *Mar Policy* 2009;33:635–42. doi: <https://doi.org/10.1016/j.marpol.2008.12.013>.
- [143] Rozlan MBM, Zobaa AF, Abdel Aleem SHE. The optimisation of stand-alone hybrid renewable energy systems using HOMER. *Int Rev Electr Eng* 2011;6:1802–10.
- [144] Eshra NM, Zobaa AF, Abdel Aleem SHE. Assessment of mini and micro hydropower potential in Egypt: multi-criteria analysis. *Energy Rep* 2021;7:81–94. doi: <https://doi.org/10.1016/j.egypro.2020.11.165>.
- [145] Savari GF, Sathik MJ, Raman LA, El-Shahat A, Hasanien HM, Almakhlis D, et al. Assessment of charging technologies, infrastructure and charging station recommendation schemes of electric vehicles: a review. *Ain Shams Eng J* 2023;14:. doi: <https://doi.org/10.1016/j.asej.2022.101938>.



**Ahmed Mahdy** received the B.Sc. degree in electrical power engineering in 2018 from the Ain Shams University, Faculty of Engineering, Cairo, Egypt, where he is currently working toward the M.Sc. degree. He is currently an Electrical Instructor having more than 56,000 students in more than 170 countries on 23 online course platforms that include Udemy, Skillshare, StackSkills, EEP, and StackCommerce, in addition to his own website Khadija Academy. His research interests include modern control techniques, renewable energy systems, power systems dynamics, energy storage systems, and smart grid.



**Hany M. Hasanien** (Senior Member, IEEE) received the B.Sc., M.Sc., and Ph.D. degrees in electrical engineering from the Faculty of Engineering, Ain Shams University, Cairo, Egypt, in 1999, 2004, and 2007, respectively. From 2008 to 2011, he was a Joint Researcher with the Kitami Institute of Technology, Kitami, Japan. From 2012 to 2015, he was Associate Professor with the College of Engineering, King Saud University, Riyadh, Saudi Arabia. He is currently a Professor with the Electrical Power and Machines Department, Faculty of Engineering, Ain Shams University. He has authored or coauthored, and edited three books in the field of electric machines and renewable energy. He has authored or coauthored more than 200 papers in international journals and conferences. His research interests include modern control techniques, power systems dynamics and control, energy storage systems, renewable energy systems, and smart grid. He is an Editorial Board Member of *Electric Power Components and Systems Journal*. He the Subject Editor of the *IET Renewable Power Generation*, *Frontiers in Energy Research*, and *Electronics MDPI*. His biography has been included in *Marquis Who's Who in the world* for its 28 edition, 2011. He was awarded the Encouraging Egypt Award for Engineering Sciences in 2012. He was awarded the Institutions Egypt Award for Invention and Innovation of Renewable Energy Systems Development in 2014. He was awarded the Superiority Egypt Award for Engineering Sciences in 2019. He is currently the IEEE PES Egypt Chapter Chair and is the Editor in Chief of *Ain Shams Engineering Journal*.



**Shady H. E. Abdel Aleem** (M'12, SM'21) received B.Sc., M.Sc., and Ph.D. degrees in Electrical Power and Machines from the Faculty of Engineering, Helwan University, Egypt, in 2002, and the Faculty of Engineering, Cairo University, Egypt, in 2010 and 2013 respectively. Currently, he is an Associate Professor at the Department of Electrical Engineering Institute of Aviation Engineering and Technology, Egypt. Also, he is a consultant of power quality studies in ETA Electric Company, Egypt. His research interests include harmonic problems in power systems, power quality, renewable energy, smart grid, energy efficiency, optimization, green energy, and economics. Dr. Shady is the author or co-author of many refereed journals and conference papers. He has published 180 plus journal and conference papers, 20 plus book chapters, and 10 edited books with the Institution of Engineering and Technology (IET), Elsevier, Springer, CRC Press, and InTech. He was awarded the State Encouragement Award in Engineering Sciences in 2017 from Egypt. He was also awarded the medal of distinction from the first class of the Egyptian State Award in 2020 from Egypt. Dr. Shady is a senior member of the Institute of Electrical and Electronics Engineers (IEEE). Dr. Shady is also a member of the Institution of Engineering and Technology (IET). He is an Editor/Guest Editor/Associate Editor for the International Journal of Renewable Energy Technology, Vehicle Dynamics, IET Journal of Engineering, Energies, Sustainability, Technology and Economics of Smart Grids and Sustainable Energy, and Others.



**Mujahed Al-Dhaifallah** received the B.Sc. and M.Sc. degrees in systems engineering from King Fahd University of Petroleum & Minerals, Dhahran, Saudi Arabia, and a Ph.D. degree in electrical and computer engineering from the University of Calgary, Calgary, AB, Canada. Currently, he is an Associate Professor of Control & Instrumentation Engineering at King Fahd University of Petroleum & Minerals. His current research interests include nonlinear systems identification, control systems, optimization, artificial intelligence, and renewable energy.



**Ahmed F. Zobaa** (Senior Member, IEEE) received B.Sc. (Hons.), M.Sc., and Ph.D. degrees in electrical power and machines from Cairo University, Cairo, Egypt, in 1992, 1997, and 2002, respectively. Between 2007 and 2010, he was a Senior Lecturer in renewable energy with the University of Exeter, Exeter, U.K. He was also an Instructor with Cairo University between 1992 and 1997, a Teaching Assistant between 1997 and 2002, an Assistant Professor between 2003 to 2008, and an Associate Professor from 2008 and 2013, where he has also been a Professor (on leave) since December 2013. He is currently a Reader in power systems and a Full Member of the Institute of Energy Futures, Brunel University London, London, U.K. His main areas of expertise are power quality, (marine) renewable energy, smart

grids, energy efficiency, and lighting applications. Dr. Zobaa is currently a Senior Fellow of the Higher Education Academy of U.K., and a Fellow of the IET, the Energy Institute of the U.K., the Chartered Institution of Building Services Engineers, the Institution of Mechanical Engineers, the Royal Society of Arts, the African Academy of Science, and the Chartered Institute of Educational Assessors. He is a member of the International Solar Energy Society, the European Power Electronics and Drives Association, and the IEEE Standards Association. He is the Editor-in-Chief for the International Journal of Renewable Energy Technology, International Journal of Electrical Engineering & Education, and Technology and Economics of Smart Grids and Sustainable Energy. He is also an Editorial Board member, Editor, Associate Editor, and Editorial Advisory Board member for many international journals. He is a registered Chartered Engineer, Chartered Energy Engineer, European Engineer, and International Professional Engineer, and is a registered member of the Engineering Council U.K., Egypt Syndicate of Engineers, and the Egyptian Society of Engineers.



sity, Saudi Arabia.

**Ziad M. Ali** received the B.Sc. degree in electrical engineering from Assiut University, faculty of engineering, Assuit, Egypt, in 1998. He worked as a demonstrator in Aswan faculty of engineering, south valley university, Aswan, Egypt. He obtained an M.Sc. degree from Assiut University, faculty of engineering in electrical engineering in 2003. He worked as Assistant Lecturer in Aswan faculty of Engineering. He obtained a Ph.D. degree in 2010 from Kazan State Technical University, Tatarstan, Russia. He is currently working as Associate Professor in Electrical Dept. College of Engineering at Wadi Addawasir, Prince Sattam bin Abdulaziz Univer-